JACS
JOURNAL OF THE AMERICAN CHEMICAL SOCIETY

pubs.acs.org/JACS

Article

Cobalt(III) Carbene Complex with an Electronic Excited-State Structure Similar to Cyclometalated Iridium(III) Compounds

Narayan Sinha, Björn Pfund, Christina Wegeberg, Alessandro Prescimone, and Oliver S. Wenger*

Cite This: J. Am. Chem. Soc. 2022, 144, 9859−9873

Read Online

ACCESS | Metrics & More | Article Recommendations | Supporting Information

ABSTRACT: Many organometallic iridium(III) complexes have photoactive excited states with mixed metal-to-ligand and intraligand charge transfer (MLCT/ILCT) character, which form the basis for numerous applications in photophysics and photochemistry. Cobalt(III) complexes with analogous MLCT excited-state properties seem to be unknown yet, despite the fact that iridium(III) and cobalt(III) can adopt identical low-spin d^6 valence electron configurations due to their close chemical relationship. Using a rigid tridentate chelate ligand (L^{CNC}), in which a central amido π-donor is flanked by two σ-donating N-heterocyclic carbene subunits, we obtained a robust homoleptic complex $[Co(L^{CNC})_2](PF_6)$, featuring a photoactive excited state with substantial MLCT character. Compared to the vast majority of isoelectronic iron(II) complexes, the MLCT state of $[Co(L^{CNC})_2](PF_6)$ is long-lived because it does not deactivate as efficiently into lower-lying metal-centered excited states; furthermore, it engages directly in photoinduced electron transfer reactions. The comparison with $[Fe(L^{CNC})_2](PF_6)$, as well as structural, electrochemical, and UV−vis transient absorption studies, provides insight into new ligand design principles for first-row transition-metal complexes with photophysical and photochemical properties reminiscent of those known from the platinum group metals.

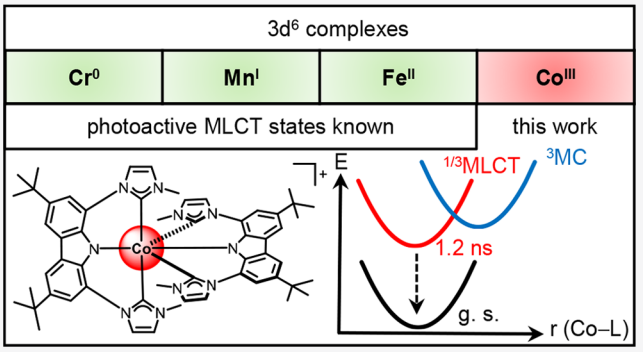

INTRODUCTION

Coordination complexes and organometallic compounds of ruthenium(II) and iridium(III) are among the most widely used substance classes for applications in lighting,[1,2] sensing,[3] photocatalysis,[4−9] upconversion,[10,11] solar energy conversion, and phototherapy.[12−18] Research on precious-metal-based compounds continues to be important because they are comparatively robust and often promise excellent performance.[19−35] Nevertheless, there is now an increasing interest in photoactive complexes made from first-row transition metals.[36,37] Higher abundance and lower cost are often quoted as key motivators for research in this direction,[38] but aside from such practical aspects, there is still much room for fundamental and groundbreaking discovery in the photophysics and the photochemistry of first-row transition-metal complexes.[39−44]

Complexes with semiprecious copper(I) have been investigated particularly thoroughly.[45−56] Given their filled $3d^{10}$ subshell, long-lived excited states are far more easily established in copper(I) complexes than in complexes with a partially filled 3d subshell because there are no low-lying metal-centered (MC) states that facilitate undesired nonradiative excited-state relaxation. Among first-row transition-metal compounds with partially filled d-orbitals, six-coordinate chromium(III) complexes are popular[57] because the lowest spin-flip MC state of octahedral d^3 complexes is only weakly distorted relative to the electronic ground state, which is helpful to obtain unusually long-lived luminescence.[58−62] By contrast, MLCT excited states of nickel(II) ($3d^8$)[63−66] and iron(II) ($3d^6$)[44,67−71] complexes typically deactivate very rapidly, making it very difficult to use these compounds for similar applications as second- or third-row d^8 and d^6 metal complexes, in which long-lived MLCT states govern the photophysics and the photochemistry.[67−73]

Photoactive iron(II) complexes have been investigated for several decades, with much focus on excited-state deactivation pathways,[74−76] the establishment of longer-lived MLCT states,[77−83] and the use of such compounds in photoredox catalysis.[84−87] By contrast, the photophysics and photochemistry of isoelectronic cobalt(III) complexes have received surprisingly little attention, and the comparatively few examples investigated in detail until now either have photoactive MC or ligand-to-metal charge transfer (LMCT) excited states.[88,89] Here, we disclose an organometallic cobalt(III) complex featuring a photoactive excited state with

Received: March 9, 2022
Published: May 27, 2022

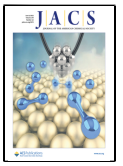

https://doi.org/10.1021/jacs.2c02592
J. Am. Chem. Soc. 2022, 144, 9859−9873

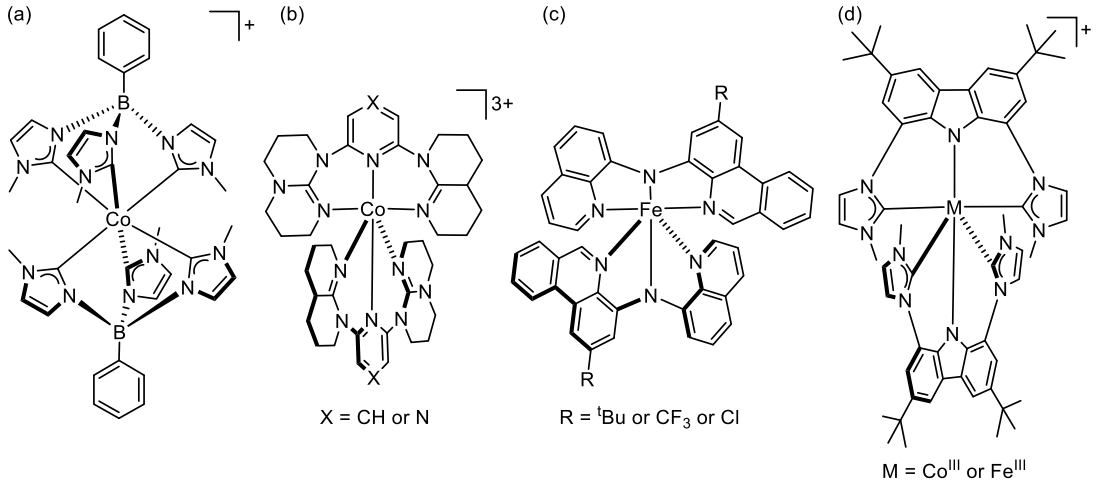

Figure 1. Molecular structures of previously investigated pertinent complexes along with the compounds investigated herein. (a) Cobalt(III) complex emitting from an MC state;[88] (b) cobalt(III) complex emitting from an excited state with substantial LMCT character;[89] (c) iron(II) complex with amido π-donor ligand units;[78,96] (d) new $[Co(L^{CNC})_2]^+$ and $[Fe(L^{CNC})_2]^+$ compounds investigated herein.

substantial MLCT character, similar to what is well known from many cyclometalated iridium(III) compounds. This MLCT excited state does not relax as efficiently into lower-lying MC states as is typically observed in isoelectronic iron(II) complexes,[36,55−57,74−85,90−95] and it can undergo photoinduced electron transfer in an analogous fashion as many ruthenium(II) and iridium(III) complexes.

The higher oxidation state of cobalt(III) with respect to isoelectronic iron(II) causes a stronger ligand field, and this is helpful in terms of suppressing unwanted nonradiative relaxation from distorted MC excited states.[17,97] Owing to the particularly strong ligand field of $[Co(CN)_6]^{3-}$, its lowest MC state ($^3T_1$) is sufficiently high in energy for luminescence to become a competitive deactivation pathway.[98,99] Building on these early findings, the use of an anionic tripodal borate ligand with three strongly σ-donating carbene subunits recently led to a cobalt(III) complex with enhanced luminescence properties from that $^3T_1$ state (Figure 1a).[88] In separate studies by other investigators who used tridentate imine σ-donor ligands, two cobalt(III) complexes featuring emission from a state with substantial LMCT character were obtained (Figure 1b),[89] contributing to the recent surge of interest in LMCT luminophores and photocatalysts.[100−109]

In our work aiming at cobalt(III) complexes with a photoactive MLCT state, it seemed desirable to explore ligands that increase the electron density at the metal center (to lower the $Co^{IV/III}$ potential). Furthermore, it seemed necessary to have ligands with low-lying π^* orbitals (as landing spots for MLCT-excited electrons) while maintaining a strong ligand field (to shift MC states to higher energies). In recently explored iron(II) complexes, amido π-donor ligands markedly lowered the metal oxidation potential (Figure 1c),[78,96] and therefore, we focused on a tridentate ligand (Figure 1d), in which a central anionic carbazolate bears two N-heterocyclic carbene units (L^{CNC}). This chelate ligand follows the abovementioned design principles; furthermore, it can potentially provide rigid coordination of cobalt(III) with bond angles close to ideal octahedral symmetry, which is known to counteract unwanted nonradiative relaxation.[37,57,110,111] Until now, this ligand (L^{CNC}) had been used for square-planar d^8 complexes based on rhodium(I),[112] iridium(I),[113] nickel(II),[114] palladium(II),[114,115] and platinum(II),[114] mostly in contexts not related to photophysics, except for platinum(II) alkynyl compounds with luminescent MLCT states.[116,117] Although the main focus of our work was on cobalt(III), it seemed useful to explore at the same time an isostructural iron(III) complex as a reference compound. Indeed, the comparative investigation of the $3d^6$ and $3d^5$ compounds $[Co(L^{CNC})_2](PF_6)$ and $[Fe(L^{CNC})_2](PF_6)$ provides insight into new ligand design principles for first-row transition-metal complexes with photophysical and photochemical properties reminiscent of those known from precious metal compounds.

RESULTS AND DISCUSSION

Synthesis and Characterization of the Complexes. The ligand precursor $(H_3L^{CNC})(PF_6)_2$ was synthesized via an anion exchange reaction from $(H_3L^{CNC})(I)_2$. The latter compound was prepared by adapting a previously published procedure (see Supporting Information Page S3).[114] The reaction of 1 equiv of $(H_3L^{CNC})(PF_6)_2$ and 0.5 equiv of $CoCl_2$ or $FeBr_2$ in the presence of 3.3 equiv of potassium *tert*-butoxide in tetrahydrofuran at 55 °C for 18 h, followed by subsequent oxidation under air, resulted in the formation of the $[Co(L^{CNC})_2](PF_6)$ and $[Fe(L^{CNC})_2](PF_6)$ compounds (Scheme 1) as orange and green solids, respectively. Both substances are insensitive to air and moisture.

The diamagnetic cobalt(III) compound was characterized by NMR spectroscopy, mass spectrometry, combustion analysis, and X-ray crystallography (Supporting Information Page S4). Upon formation of $[Co(L^{CNC})_2](PF_6)$, the characteristic N−H proton and the (N)C−H(N) protons of the imidazolium groups of $(H_3L^{CNC})(PF_6)_2$ at 11.45 and 9.72 ppm, respectively, are no longer observable in the ^1H NMR spectrum. Instead, a new resonance appears at 172.0 ppm in the ^{13}C NMR spectrum of $[Co(L^{CNC})_2](PF_6)$, attributable to the ligating carbon atom of the *N*-heterocyclic carbene (NHC) units, in line with previously reported cobalt(III)-NHC complexes.[88] Orange-colored single crystals of $[Co(L^{CNC})_2](PF_6)\cdot 2C_2H_4Cl_2$ suitable for an X-ray diffraction study were obtained by slow vapor diffusion of pentane into a saturated 1,2-dichloroethane solution of $[Co(L^{CNC})_2](PF_6)$ at ambient temperature. Structure analysis confirmed the formation of the expected diamidotetracarbene cobalt(III) complex cation $[Co(L^{CNC})_2]^+$

https://doi.org/10.1021/jacs.2c02592
J. Am. Chem. Soc. 2022, 144, 9859−9873

Scheme 1. Synthesis of the Cobalt(III) and Iron(III) Compounds Investigated Herein

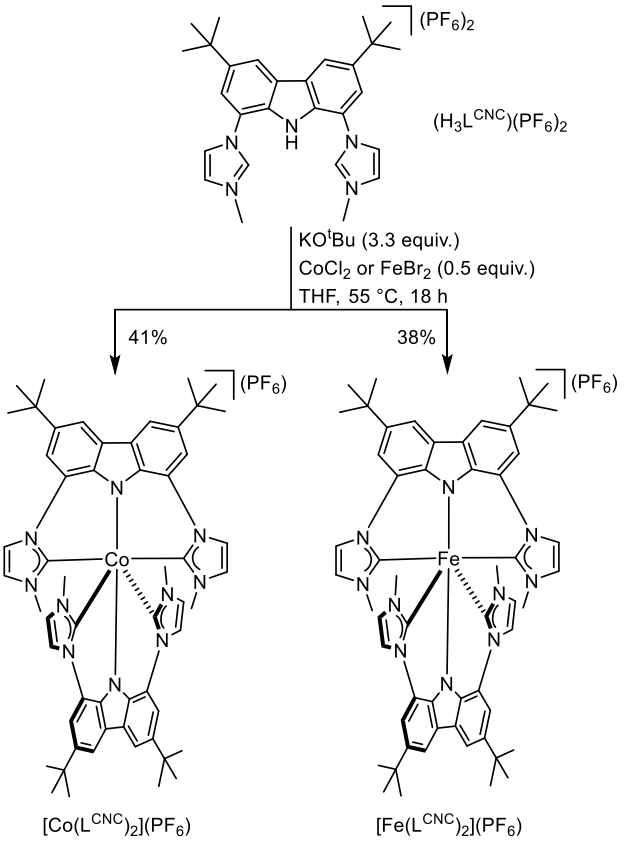

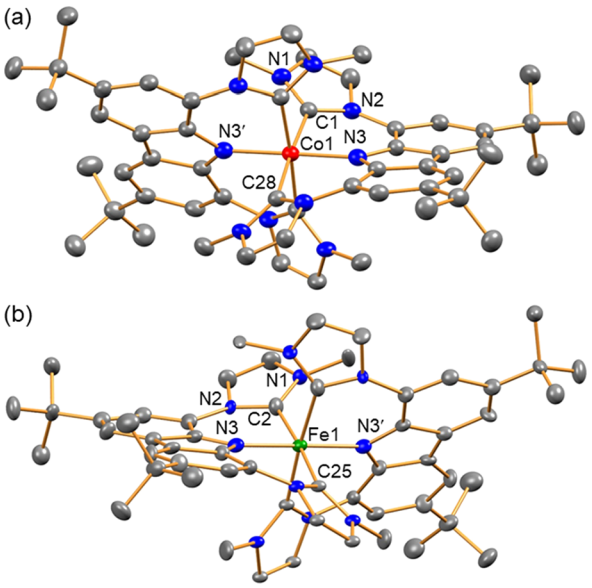

Figure 2. Molecular structures of the complex cations in $[Co(L^{CNC})_2](PF_6)\cdot 2C_2H_4Cl_2$ (a) and in $[Fe(L^{CNC})_2](PF_6)\cdot 2C_2H_4Cl_2$ (b); 50% probability ellipsoids used in both cases. Hydrogen atoms, the counter anion, and the solvent molecules have been omitted for clarity. Selected bond lengths (Å) and angles (°) for $[Co(L^{CNC})_2]^+$: Co1−C1, 1.997(4); Co1−C28, 2.000(4); Co1−N3, 1.910(3); C1−Co1−C28, 176.67(14)°; N3−Co1−N3′, 179.5(2); and for $[Fe(L^{CNC})_2]^+$: Fe1−C2, 2.016(5); Fe1−C25, 2.013(4); Fe1−N3, 1.910(4); C2−Fe−C25, 175.9(2)°; N3−Fe−N3′, 179.6(2)°. Different enantiomers are shown for the two complexes.

(Figure 2a), which has a close-to-perfect octahedral geometry around the cobalt(III) center. The $N_{amido}-Co-N_{amido}$ bond angle is 179.5(2)°, and the $C_{NHC}-Co-C_{NHC}$ bond angle is 176.67(14)°. The $Co-N_{amido}$ bond length (1.910(3) Å) is shorter than the $Co-C_{NHC}$ bond lengths (1.997(4) and 2.000(4) Å), and this is compatible with the more covalent character of the $Co-N_{amido}$ bond in the present Co^{III} complex.[96,118] The two imidazolidene rings in L^{CNC} are not coplanar but rather tilted from the central carbazole plane, and hence, the L^{CNC} ligand adopts a helical twist compatible with *P* or *M* chirality according to Cahn−Ingold−Prelog notation.[119] In the crystal structure, the Co^{III} complex cation exists as a pair of *PP*-$[Co(L^{CNC})_2]^+$/*MM*-$[Co(L^{CNC})_2]^+$ enantiomers, similar to recently reported Cr^{III} complexes.[59,62,118,120]

The paramagnetic $[Fe(L^{CNC})_2](PF_6)$ compound was characterized by combustion analysis, high-resolution electrospray ionization (HR-ESI) mass spectrometry, EPR spectroscopy, and X-ray crystallography (Supporting Information Page S5). The X-band EPR spectrum of $[Fe(L^{CNC})_2](PF_6)$ in acetonitrile at 77 K shows a broad isotropic signal with a *g*-value of 2.07 (Figure S1), compatible with the low-spin d^5 valence electron configuration that was previously observable for related iron(III) compounds.[41,78,107,121] Green-colored single crystals of $[Fe(L^{CNC})_2](PF_6)\cdot C_2H_4Cl_2$ suitable for an X-ray diffraction study were grown by slow vapor diffusion of pentane into a saturated 1,2-dichloroethane solution of $[Fe(L^{CNC})_2](PF_6)$ at ambient temperature. Structure analysis revealed the near-perfect octahedral structure of the diamidotetracarbene iron(III) complex cation $[Fe(L^{CNC})_2]^+$ (Figure 2b). Analogously to $[Co(L^{CNC})_2]^+$, in $[Fe(L^{CNC})_2]^+$, the metal−N_{amido} bond length (1.910(4) Å) is shorter than the metal−C_{NHC} bond lengths (2.013(4) and 2.016(5) Å). Key bond lengths and angles are in the expectable range of values according to previously published iron(III) complex structures containing $Fe-N_{amido}$ or $Fe-C_{NHC}$ bonds.[78,107] Similar to $[Co(L^{CNC})_2]^+$, $[Fe(L^{CNC})_2]^+$ also exists as *PP*- and *MM*-enantiomers in the crystal structure.

Electrochemistry. Two reversible oxidation waves appear in the cyclic voltammogram of $[Co(L^{CNC})_2](PF_6)$ recorded in acetonitrile with 0.1 M tetra-*n*-butylammonium hexafluorophosphate ($^nBu_4N)(PF_6$) at 22 °C (Figure 3a). The first oxidation wave at 0.42 V versus $Fc^{+/0}$ is attributed to the $Co^{IV/III}$ couple based on a comparison with a recently reported (less electron-rich) cobalt(III)−hexacarbene complex (Figure 1a), in which the $Co^{IV/III}$ redox couple appeared at 0.96 V versus $Fc^{+/0}$ (entry 2 of Table 1).[88] This shift of the $Co^{IV/III}$ potential to a substantially less positive value is attributed to the combined σ- and π-donor properties of the L^{CNC} ligand, including the anionic nature of the carbazolate subunit,[112] and this is further supported below by additional experimental results and computational studies. The second oxidation wave at 0.72 V versus $Fc^{+/0}$ is ascribed to ligand oxidation in the $[Co(L^{CNC})_2]^+$ complex, whereas the irreversible wave at −2.21 V versus $Fc^{+/0}$ in Figure 3a is attributed to ligand reduction. Unlike in cobalt(III) complexes with less electron-rich ligands,[89,122,123] a $Co^{III/II}$ redox wave is not detectable for $[Co(L^{CNC})_2](PF_6)$ in the electrochemical window of acetonitrile.[124] Further experimental evidence that the first oxidation of $[Co(L^{CNC})_2]^+$ is a metal-centered $Co^{IV/III}$ process is given in the Supporting Information (Figure S18b).

In the cyclic voltammogram of $[Fe(L^{CNC})_2](PF_6)$ recorded under identical conditions (Figure 3b), the first oxidation wave appears at 0.05 V versus $Fc^{+/0}$. This is in line with the potential

https://doi.org/10.1021/jacs.2c02592
J. Am. Chem. Soc. 2022, 144, 9859−9873

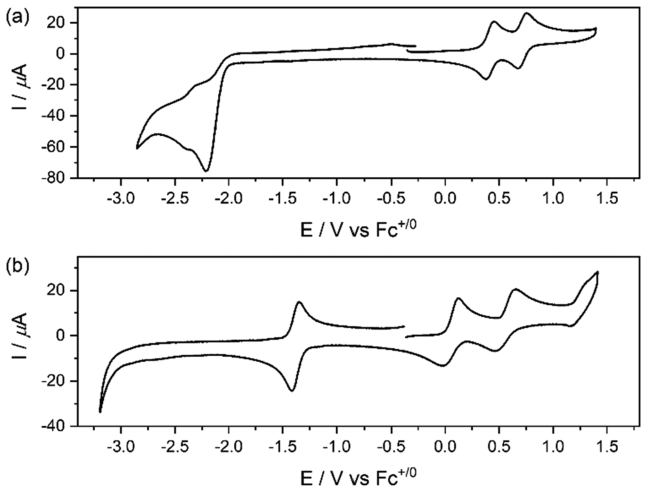

Figure 3. Cyclic voltammograms of (a) 1 mM $[Co(L^{CNC})_2](PF_6)$ and (b) 1 mM $[Fe(L^{CNC})_2](PF_6)$ in deaerated acetonitrile at 22 °C. 0.1 M ($^nBu_4N$) (PF_6) was used as the electrolyte, and the potential scan rate was 0.1 V/s in both cases.

reported for the $Fe^{IV/III}$ redox couple in a related iron(III) complex (entry 4 of Table 1)[121] and consequently is attributed to a metal-centered oxidation event. The second oxidation wave appearing at 0.56 V versus $Fc^{+/0}$ is attributed to ligand oxidation (entry 3 of Table 1), which appears to be cathodically shifted by 0.16 V relative to the cobalt(III) complex. A metal-based oxidation process leading to iron(V) does not seem plausible in this case here.[125] On the reductive side, the $Fe^{III/II}$ redox couple is readily detectable at −1.38 V versus $Fc^{+/0}$, in line with the potentials reported for two iron(III) complexes with related coordination environments (entries 4 & 5 in Table 1).[107,121] The fact that the first reduction event in $[Fe(L^{CNC})_2](PF_6)$ is metal-centered and leads to iron(II) then evidently precludes the detection of the same ligand-centered reduction event as for the isostructural cobalt(III) complex, at least in acetonitrile.

Turning our attention back to the $[Co(L^{CNC})_2](PF_6)$ compound, we note that the first oxidation event is metal-based, whereas the first reduction process is ligand-centered. Based on the relevant $Co^{IV/III}$ and $L^{0/\bullet-}$ potentials of 0.42 and −2.21 V versus $Fc^{+/0}$ (entry 1 of Table 1), respectively, one can expect an MLCT excited-state energy of approximately 2.6 eV. Furthermore, given a ligand-centered oxidation at 0.72 V versus $Fc^{+/0}$, an intraligand charge transfer (ILCT) excited state can be anticipated at roughly 2.9 eV. The combined experimental and computational studies presented in the following will demonstrate that these two expectations regarding the lowest MLCT and ILCT states are largely fulfilled.

UV−Vis Absorption Spectroscopy. The $(H_3L^{CNC})(PF_6)_2$ ligand precursor is optically transparent over large parts of the visible spectrum but features several $\pi-\pi^*$ absorption bands at wavelengths shorter than 450 nm (Figure 4a). The $[Co(L^{CNC})_2]^+$ complex (Figure 4b) exhibits a pronounced absorption band with a maximum at 430 nm and a molar extinction coefficient (ε_{430}) of 14,000 M^{-1} cm^{-1}, which is substantially greater than twice the ε_{430} value of the $(H_3L^{CNC})(PF_6)_2$ ligand precursor (2 × 2200 M^{-1} cm^{-1}). It follows that the longest-wavelength UV−vis absorption band of $[Co(L^{CNC})_2](PF_6)$ is most likely due to a different type of electronic transition than in the ligand precursor. The onset of the respective band is near 450 nm, which corresponds to 2.75 eV and thus falls into the range, in which MLCT and ILCT transitions are expectable on the basis of the electrochemical investigations. Time-dependent density functional theory (TD-DFT) calculations support this interpretation and suggest that the absorption band at 430 nm is caused by a transition with substantial MLCT character (transition 3 in Table S3), whereas the shoulder at 408 nm (transition 9 in Table S3) is predominantly of ILCT type (vertical bars in Figure 4b, see Supporting Information Page S24 for details). The energy difference between these two absorption bands is 0.16 eV, which seems reasonably close to the value of 0.3 eV estimated on the basis of the redox potentials in Table 1.[126] The calculated difference electron density plot for the lowest-energy transition (Figure 4d) illustrates its substantial MLCT character, showing depletion of electron density (colored in purple) at the metal center and the amido N atoms, along with an increase of electron density (colored in light blue) at the NHC moieties (in particular the ligating C atoms) and the carbazole backbone. For fragment contributions and a more detailed discussion of the HOMO−LUMO transition, see Tables S4/S5 in the Supporting Information.

$[Fe(L^{CNC})_2](PF_6)$ shows multiple absorption bands in the blue−green and in the red spectral range (Figure 4c), similar to recently reported iron(III) and iron(II) compounds,[78,96,121] for which the concept of "HOMO inversion" was put forward.[127] Applied to the $[Fe(L^{CNC})_2]^+$ complex, this concept would predict that the filled amido N(2p) orbitals mix with the occupied metal 3d-orbitals, resulting in a HOMO of combined metal−ligand character at somewhat more elevated energy than the pure iron-based 3d orbitals in the absence of mixing. Such metal−ligand orbital mixing is indeed what we have found (Figure 4d) for the lowest-energy transition of

Table 1. Electrochemical Potentials ($E_{1/2}$ in V vs $Fc^{+/0}$) of $[Co(L^{CNC})_2](PF_6)$, $[Fe(L^{CNC})_2](PF_6)$, and a Few Pertinent NHC Complexes of Cobalt(III) and Iron(III)

entry	compound	$E_{1/2}(M^{IV/III})$[a]	$E_{1/2}(L^{\bullet+/0})$	$E_{1/2}(L^{0/\bullet-})$	$E_{1/2}(Fe^{III/II})$
1	$[Co(L^{CNC})_2]^+$[b]	0.42	0.72	−2.21[c]	N/A
2	$[Co(PhB(MeIm)_3)_2]^+$[d]	0.96	1.55		N/A
3	$[Fe(L^{CNC})_2]^+$[b]	0.05	0.56		−1.38
4	$[Fe(ImP)_2]^+$[e]	0.08	1.23		−1.16
5	$[Fe(phtmeimb)_2]^+$[f]	0.25	1.67[c]		−1.16
6	$[Fe(btz)_3]^{3+}$[g]		1.16[c]		−0.58

[a]M = Co or Fe. [b]This work. [c]Irreversible wave. [d]$PhB(MeIm)_3$ = tris(3-methylimidazolin-2-ylidene) (phenyl)borate (Figure 1a).[88] [e]Imp = deprotonated form of 1,1′-(1,3-phenylene)bis(3-methyl-1-imidazol-2-ylidene).[121] [f]Phtmeimb = phenyl[tris(3-methylimidazol-1-ylidene)]borate.[107] [g]Btz = 3,3′-dimethyl-1,1′-bis(*p*-tolyl)-4,4′-bis(1,2,3-triazol-5-ylidene).[41]

https://doi.org/10.1021/jacs.2c02592
J. Am. Chem. Soc. 2022, 144, 9859−9873

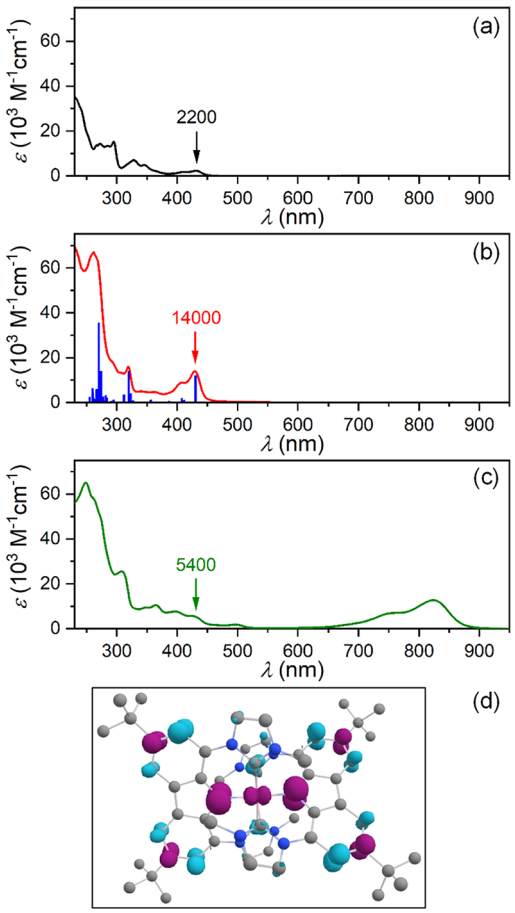

Figure 4. UV−vis absorption spectra of the (a) ligand precursors $(H_3L^{CNC})(PF_6)_2$, (b) $[Co(L^{CNC})_2](PF_6)$, and (c) $[Fe(L^{CNC})_2](PF_6)$ in acetonitrile at 22 °C. Molar extinction coefficients at 430 nm (ε_{430} in units of M^{-1} cm^{-1}) are indicated. The blue bars (Figure 4b) mark the energies of TD-DFT-calculated vertical transitions for the Co^{III} complex, and the heights of these bars reflect relative oscillator strengths. (d) Electron density difference plot for the lowest-energetic transition of $[Co(L^{CNC})_2](PF_6)$ at 430 nm with a high oscillator strength of 0.224, based on TD-DFT calculations, with purple color marking a depletion and light-blue color indicating a gain of electron density.

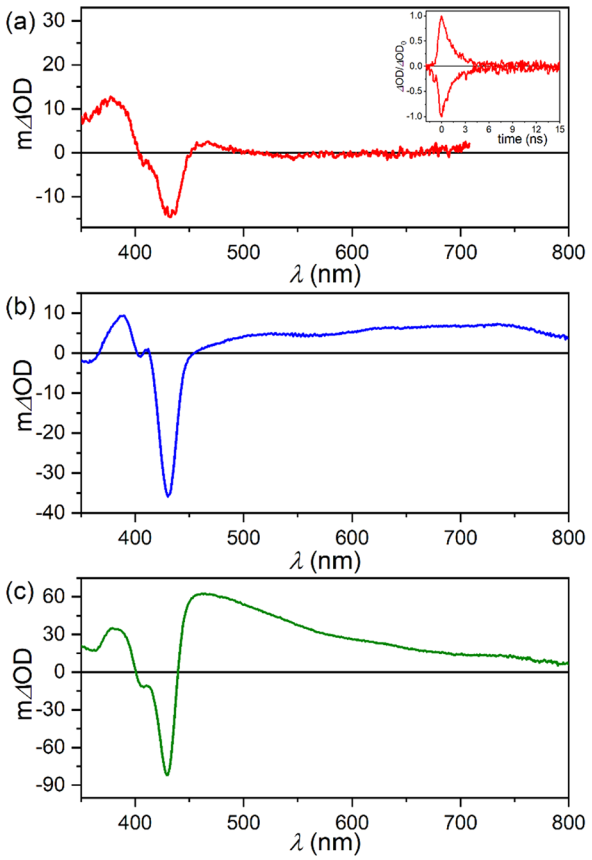

Figure 5. (a) Picosecond transient absorption spectrum of 100 μM $[Co(L^{CNC})_2](PF_6)$ in deaerated acetonitrile at 22 °C obtained after excitation at 430 nm, time-integrated over 2 ns. The inset in the upper right corner shows the decay of the ESA signal at 380 nm and the recovery of the ground-state absorption bleach at 430 nm (both decay traces normalized to a ΔOD value of 1 at time = 0). (b) UV−vis absorption changes following metal-based oxidation of $[Co(L^{CNC})_2](PF_6)$ at 0.42 V versus $Fc^{+/0}$ [= $E_{1/2}(Co^{IV/III})$] in acetonitrile at 22 °C. (c) UV−vis absorption changes upon ligand-centered reduction of $[Co(L^{CNC})_2](PF_6)$ at −2.3 V versus $Fc^{+/0}$ (<$E_{1/2}(L^{0/\bullet-})$) in deaerated acetonitrile at 22 °C. The electrolyte was 0.1 M (^{n}Bu$_4$N)(PF_6) in both spectro-electrochemical experiments.

$[Co(L^{CNC})_2](PF_6)$. In $[Fe(L^{CNC})_2](PF_6)$, there are additional absorption bands between 600 and 900 nm, which are likely due to LMCT transitions, expectable near 1.94 eV (639 nm) based on the electrochemical data in Table 1 ($E_{1/2}(L^{\bullet+/0})$ − $E_{1/2}(Fe^{III/II})$).

Transient Absorption and Excited-State Dynamics. The combination of picosecond UV−vis transient absorption spectroscopy with spectro-electrochemical investigations further corroborates the substantial MLCT character of the lowest excited state of $[Co(L^{CNC})_2](PF_6)$, as seen in the following. Upon excitation at 430 nm with a picosecond laser, the UV−vis transient absorption difference spectrum shown in Figure 5a is obtained, featuring the disappearance of the lowest-energy ground-state absorption band at 430 nm, along with an excited-state absorption (ESA) band peaking at 380 nm and a weaker ESA band near 460 nm. The overall appearance of this spectrum is similar to the transient absorption difference spectrum known from ^{3}MLCT-excited ruthenium(II) polypyridine complexes, which includes essentially the same two ESA bands (in similar intensity ratio) in combination with the MLCT bleach.[128−130] Spectro-electrochemistry at a potential of 0.42 V versus $Fc^{+/0}$ (inducing oxidation of cobalt(III) to cobalt(IV) according to Table 1) yields the UV−vis difference spectrum presented in Figure 5b, for which the UV−vis absorption spectrum prior to applying any potential served as a baseline. The disappearance of the lowest-energy absorption band of $[Co(L^{CNC})_2]^+$ at 430 nm is evident, whereas the $[Co(L^{CNC})_2]^{2+}$ complex has prominent absorption bands near 380 nm and in the red spectral range (even beyond the accessible spectral region of the picosecond transient absorption experiment of Figure 5a). Reductive spectro-electrochemistry was performed in an analogous manner by applying a potential of −2.3 V versus $Fc^{+/0}$, which leads to ligand reduction according to Table 1. The 430 nm band of $[Co(L^{CNC})_2]^+$ also disappears under these conditions (Figure 5c), whereas $[Co(L^{CNC})(L^{CNC})^{\bullet-}]$ features prominent absorptions near 380 and 460 nm. The UV−vis transient absorption difference spectrum in Figure 5a is in reasonably good agreement with a 1:1 superposition of the spectro-electrochemical UV−vis difference spectra in Figure 5b/c, which monitor the effects of metal oxidation and ligand

https://doi.org/10.1021/jacs.2c02592
J. Am. Chem. Soc. 2022, 144, 9859−9873

reduction. Such good agreement strongly supports the view that the lowest-energetic excited state of $[Co(L^{CNC})_2]^+$ has substantial MLCT character.[131]

Following pulsed excitation at 430 nm, the ESA signal at 380 nm disappears with the same time constant (1.3 ns in deaerated acetonitrile at 22 °C) as the ground-state bleach at 430 nm recovers (inset of Figure 5a). This observation suggests that the lowest excited state decays directly to the electronic ground state, or at least it does not lead to a noticeable population of any MC excited state. This is an important difference to the excited-state dynamics in the vast majority of previously investigated isoelectronic iron(II) polypyridine and NHC complexes, in which the lowest MLCT state relaxes nonradiatively via lower-lying (and longer-lived) MC states.[36,55−57,74−85,90−95] Consequently, whereas photochemical reactions typically occur from MC states in iron(II) polypyridines,[84−86,132] for $[Co(L^{CNC})_2]^+$, one can expect that the MLCT state is indeed the main photoreactive excited state. It seems plausible that the stronger ligand field experienced by the more highly charged cobalt(III) in our complex (relative to isoelectronic iron(II) in various coordination environments) plays a key role in leading to this favorable behavior.

Given a lifetime of 1.3 ns for the photoactive excited state of $[Co(L^{CNC})_2](PF_6)$, radiative relaxation could in principle become a competitive decay pathway; yet our repeated attempts to detect unambiguous photoluminescence in solution at room temperature were unsuccessful. However, this MLCT state is unusually long-lived in comparison to iron(II) complexes, for which MLCT lifetimes in the picosecond time range are typical, with less than a handful of cases on (or approaching) the nanosecond timescale.[77,78,87] Owing to its comparatively long lifetime and its substantial MLCT character, the lowest excited state of $[Co(L^{CNC})_2](PF_6)$ is able to undergo photoinduced electron transfer, as demonstrated further below.

Before turning to photochemistry, however, we recall that the electrochemical, UV−vis absorption, and TD-DFT studies presented above pointed to an ILCT state at roughly 0.16−0.30 eV higher energy than the MLCT state. The results obtained by femtosecond UV−vis transient absorption spectroscopy (as presented in the following) can indeed be interpreted in terms of internal conversion (IC) from an initially coexcited ILCT to the lower-lying MLCT state. Following excitation at 430 nm, global fit analysis to the experimental UV−vis transient difference data (Figure S21) result in the two decay-associated amplitude spectra (DAS) shown in Figure 6. DAS_1 decays with a lifetime (τ_1) of 96 ± 25 ps, whereas DAS_2 has a lifetime (τ_2) of 1.24 ± 0.10 ns. The appearance of DAS_2 and its lifetime are in good agreement with the picosecond data in Figure 5a, and consequently, DAS_2 is attributable to the MLCT state discussed above. DAS_1 has a weaker bleach at 430 nm and a more pronounced ESA band at 445 nm than DAS_2 (black arrows), extending to somewhat shorter wavelengths. In a UV−vis spectro-electrochemical experiment, in which one of the ligands of $[Co(L^{CNC})_2](PF_6)$ is oxidized at a potential of 0.72 V versus $Fc^{+/0}$ [$E_{1/2}(L^{\bullet+/0})$ in Table 1], an absorption band appears quite prominently in exactly this spectral region around 445 nm (Figure S19). Furthermore, ligand reduction at −2.3 V versus $Fc^{+/0}$ [$E_{1/2}(L^{0/\bullet-})$ in Table 1] causes absorption bands around 460 nm which extend well beyond 600 nm (Figure S20). On this basis, it is tempting to attribute DAS_1 to the ILCT state and

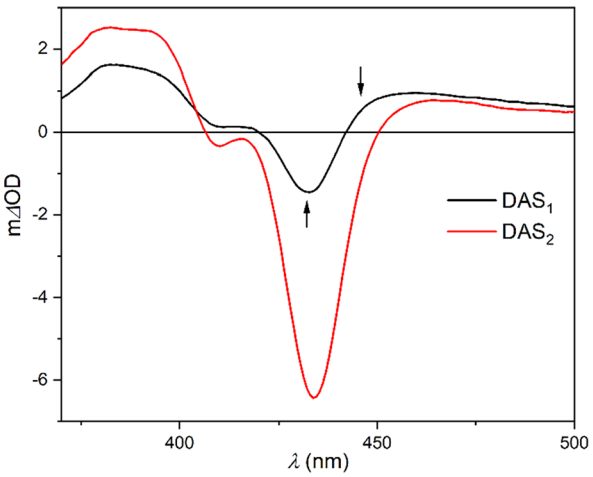

Figure 6. Decay-associated amplitude spectra (DAS) obtained from femtosecond transient absorption experiments with 260 μM (1 mm cuvette was used) $[Co(L^{CNC})_2](PF_6)$ in acetonitrile at 22 °C following excitation at 430 nm.

further conclude that τ_1 (96 ± 25 ps) reflects the kinetics for IC from the ILCT to the MLCT state. However, a timescale of roughly 100 ps seems slow in comparison to IC and other excited-state relaxation processes studied for example in nickel(II) complexes.[64,65,133,134]

Nevertheless, the combined electrochemical, UV−vis (transient) absorption, and computational studies point to the orbital picture in Figure 7a and the single-configuration

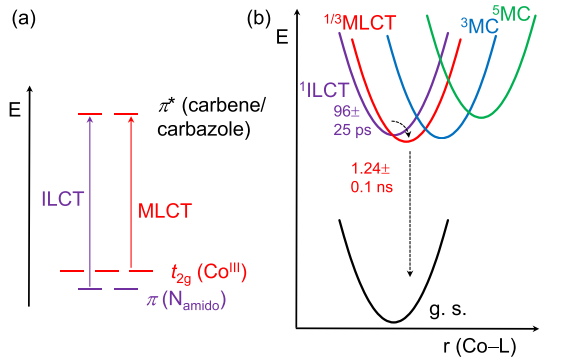

Figure 7. (a) Simplified frontier orbital picture highlighting two of the key electronic transitions occurring in $[Co(L^{CNC})_2](PF_6)$. (b) Single configurational coordinate diagram with energetically low-lying charge-transfer and MC excited states, along with the time constants of two relaxation processes. g. s. = ground state.

coordinate diagram in Figure 7b. The π^* LUMO of $[Co(L^{CNC})_2](PF_6)$ extends over the NHC moieties and the carbazole backbone of the ligands, whereas the HOMO has substantial metal character, labeled in Figure 7a simply with "t_{2g}" (thereby neglecting the contribution of amido N and other atoms seen for the HOMO−LUMO transition in Figure 4d). The HOMO − 1 is largely based on the two amido N atoms, and consequently, an ILCT transition is energetically close to the MLCT-like transition. In the potential well picture of Figure 7b, the time constant for the supposed IC from the ILCT to the $^{1/3}$MLCT state is included along with the decay time of the lowest MLCT state. The population of ^{3}MC (or even ^{5}MC)[135,136] states remains undetectable for $[Co(L^{CNC})_2](PF_6)$. If such MC states are involved in the

https://doi.org/10.1021/jacs.2c02592
J. Am. Chem. Soc. 2022, 144, 9859−9873

excited-state relaxation pathway, for example, by thermal population from the $^{1/3}$MLCT manifold, then the lifetimes of the respective MC states would have to be considerably shorter than what is often observed in isoelectronic iron(II) polypyridines.

Femtosecond UV−vis transient absorption studies of the $[Fe(L^{CNC})_2](PF_6)$ reference compound recorded after excitation at 430 nm and at 700 nm (Figures S25−S28) provide evidence for the population of a ^{2}LMCT state, in analogy to what has been recently reported for two related iron(III) compounds.[41,92,107] For $[Fe(L^{CNC})_2](PF_6)$, the lifetime of that ^{2}LMCT state in acetonitrile at 22 °C is only 1.3 ps, which is between 2 and 3 orders of magnitude shorter than in the two prior key studies.[41,107]

Photoinduced Electron Transfer. A key characteristic of MLCT excited states is their predisposition to undergo electron transfer reactions,[24,137] as nowadays widely exploited in photoredox catalysis[5−7,13,138] and in solar energy conversion.[8,9,139−144] To further corroborate the finding of a photoactive excited state with substantial MLCT character in $[Co(L^{CNC})_2](PF_6)$, it therefore seemed useful to investigate to what extent this state can indeed trigger photoinduced electron transfer reactions. Toward this end, 30 μM $[Co(L^{CNC})_2](PF_6)$ in acetonitrile was excited selectively at 430 nm in the presence of 150 mM methyl viologen hexafluorophosphate ($MV(PF_6)_2$). The resulting nanosecond UV−vis transient absorption difference spectrum in Figure 8a (green trace) shows the diagnostic spectral features of the methyl viologen radical monocation ($MV^{\bullet+}$) with maxima at 395 and 605 nm, along with a bleach around 430 nm, which coincides with the disappearing absorption band upon oxidation of cobalt(III) to cobalt(IV) in Figure 5b. Thus, the data in Figure 8a provides unambiguous evidence for photoinduced electron transfer from $[Co^{III}(L^{CNC})_2]^+$ to MV^{2+}, resulting in $[Co^{IV}(L^{CNC})_2]^{2+}$ and $MV^{\bullet+}$.

The formation of $MV^{\bullet+}$ was quantified by a relative actinometry experiment using $[Ru(bpy)_3]^{2+}$ as a reference. Specifically, an aqueous solution of $[Ru(bpy)_3]Cl_2$ and an acetonitrile solution of $[Co(L^{CNC})_2](PF_6)$ with 150 mM of $MV(PF_6)_2$ were prepared such that both solutions have identical absorbance values at the excitation wavelength (440 nm, in this case, inset of Figure 8b). The two isoabsorptive solutions were then excited at 440 nm under strictly identical conditions. The $[Ru(bpy)_3]Cl_2$ solution served to quantify the number of photons absorbed at 440 nm, whereas the $[Co(L^{CNC})_2](PF_6)/MV(PF_6)_2$ solution was used to determine the amount of $MV^{\bullet+}$ electron transfer products formed. The formation of the ^{3}MLCT excited state of $[Ru(bpy)_3]^{2+}$ occurs in a quantitative fashion and leads to a change in extinction coefficient $\Delta\varepsilon$ at 455 nm of −10,100 M^{-1} cm^{-1},[145] the well-known MLCT (ground state) bleach. By monitoring the change in optical density of the $[Ru(bpy)_3]Cl_2$ solution at 455 nm, one can therefore determine the number of photons absorbed at 440 nm, based on the (valid)[130] assumption that the ^{3}MLCT state of $[Ru(bpy)_3]^{2+}$ is the dominant photoproduct following ^{1}MLCT excitation. Since the $[Ru(bpy)_3]Cl_2$ and the $[Co(L^{CNC})_2](PF_6)/MV(PF_6)_2$ solutions both have the same optical density at 440 nm, both solutions will absorb the same number of photons under identical excitation conditions. The molar extinction coefficient ε at 395 nm for $MV^{\bullet+}$ is 41,800 M^{-1} cm^{-1};[146] hence, when monitoring the change in optical density at that wavelength, the amount of productive electron transfer events becomes quantifiable. The main plot of

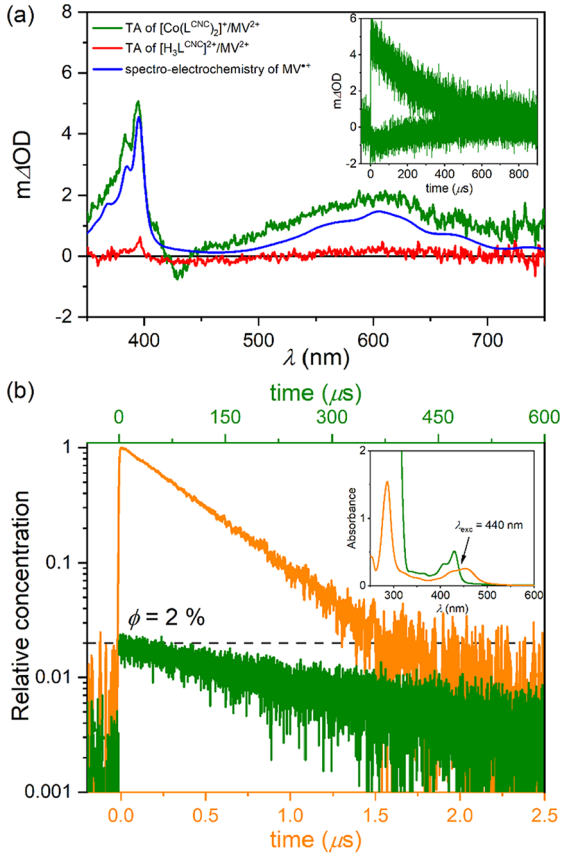

Figure 8. (a) UV−vis transient absorption difference spectra providing direct evidence for PET from $[Co(L^{CNC})_2]^+$ to MV^{2+}. In the presence of 150 mM $MV(PF_6)_2$, 30 μM $[Co(L^{CNC})_2](PF_6)$ and 110 μM ligand precursor $(H_3L^{CNC})(PF_6)_2$ were excited at 430 nm (green and red traces, respectively) with laser pulses of ca. 10 ns duration, and the signals were time-integrated over 1.5 μs with a delay time of 100 ns. The solvent was deaerated acetonitrile at 22 °C. Blue trace: UV−vis difference absorption spectrum obtained upon electrochemical reduction of MV^{2+} to $MV^{\bullet+}$ at a potential of −0.7 V versus SCE in acetonitrile. Inset: kinetic decays at 395 and 430 nm, respectively, obtained from the transient absorption spectrum (green trace) for PET from $[Co(L^{CNC})_2]^+$ to MV^{2+}, showing the disappearance of $[Co^{IV}(L^{CNC})_2]^{2+}$ and $MV^{\bullet+}$. (b) Quantum yield (ϕ) determination for the formation of $MV^{\bullet+}$ by a relative actinometry experiment as described in the main text. The orange trace reflects the ^{3}MLCT excited-state decay of $[Ru(bpy)_3]^{2+}$ upon excitation at 440 nm (monitored at 455 nm) and serves to quantify the number of absorbed photons. The green trace reflects the disappearance of $MV^{\bullet+}$, monitored at 395 nm after excitation of $[Co^{IV}(L^{CNC})_2]^+$ at 440 nm, and serves to quantify the number of productive electron transfer events. Inset: UV−vis absorption spectra of $[Co(L^{CNC})_2](PF_6)$/150 mM $MV(PF_6)_2$ in deaerated acetonitrile (green trace) and $[Ru(bpy)_3]^{2+}$ in water (orange trace), adjusted to an identical optical density at 440 nm to ensure the absorption of an equal amount of photons by both solutions.

Figure 8b shows the decays of the relative concentrations of ^{3}MLCT-excited $[Ru(bpy)_3]^{2+}$ and $MV^{\bullet+}$. Expectedly, the two photoproducts decay with very different kinetics (orange and green horizontal axes), but the key point is the relative signal intensity at time = 0, which is proportional to the relative concentrations of ^{3}MLCT-excited $[Ru(bpy)_3]^{2+}$ and $MV^{\bullet+}$ immediately after excitation. The main finding is that the quantum yield for the formation of $MV^{\bullet+}$ is about 2% (dashed black line in Figure 8b).

https://doi.org/10.1021/jacs.2c02592
J. Am. Chem. Soc. 2022, 144, 9859−9873

In general, the quantum yields for photoinduced electron transfer (PET) can depend on many different factors, among which the competition between geminate recombination and cage-escape plays a crucially important role.[147] Ruthenium(II) polypyridine complexes typically feature cage-escape yields between 5 and 60%.[148−152] Excited-state electron transfers between organic electron donors (dimethylaniline, dimethyltoluidine, and tritolylamine) and an iron(III) photosensitizer, $[Fe(phtmeimb)_2]^+$, were recently studied in detail, and it was reported that the yields for the charge-separated states are in the range of 1−7% in polar solvents such as acetonitrile and dimethylformamide.[100,107] The 2% quantum yield for the formation of the charge-separated state in our case seems much in line with these earlier findings.

Whereas the initial PET step occurs within the duration of the 10 ns laser pulses, bimolecular reverse electron transfer from $MV^{\bullet+}$ to $[Co^{IV}(L^{CNC})_2]^{2+}$ then occurs on a timescale of roughly 500 μs (inset of Figure 8a).

Photostability. Although low-spin $3d^6$ complexes along with $3d^3$ compounds are among the most substitution-inert first-row transition-metal complexes in the electronic ground state, the situation can be vastly different in some of their electronically excited states. For instance, carbonyl complexes of manganese(I) or chromium(0) ($3d^6$) undergo rapid dissociation of CO ligands upon photoexcitation,[153−155] and similarly, Cr^{III} ($3d^3$) complexes are prone to ligand dissociation in some of their distorted MC excited states.[57,156] Even well-known MLCT emitters such as $[Ru(bpy)_3]^{2+}$ and related $4d^6$/$5d^6$ luminophores undergo rather facile photodegradation,[129,157] typically as a result of the thermal population of MC states with metal−ligand dissociative character.[17,158−160] Against this background, it seemed interesting to test the inherent photostability of $[Co(L^{CNC})_2](PF_6)$ under continuous photoirradiation.

For this purpose, deaerated acetonitrile solutions of $[Co(L^{CNC})_2](PF_6)$, $[Ru(bpy)_3](PF_6)_2$, and *fac*-$[Ir(ppy)_3]$ (ppy = 2-phenylpyridine) with equal optical densities at 447 nm were prepared, and these isoabsorptive solutions were then irradiated by a continuous-wave laser with an output power of 1.1 W at that wavelength. For the emissive $[Ru(bpy)_3](PF_6)_2$ and *fac*-$[Ir(ppy)_3]$ compounds, the photoluminescence intensity was monitored directly as a function of irradiation time (red and blue lines in Figure 9), whereas for the nonemissive $[Co(L^{CNC})_2](PF_6)$ compound, UV−vis absorption spectra were recorded in time intervals of 10 min (green circles in Figure 9). Under these conditions of very intense irradiation in a coordinating solvent, $[Ru(bpy)_3]^{2+}$ decomposes nearly completely within 10 min, whereas *fac*-$[Ir(ppy)_3]$ persists for 200 min before it reaches a similar level of decomposition. In a recent study, photodegradation quantum yields of $2.76{\cdot}10^{-2}$% and $1.74{\cdot}10^{-3}$% were found for these two compounds under very similar conditions.[129] $[Co(L^{CNC})_2]^+$ remains essentially intact over the same irradiation period and no significant changes in the UV−vis absorption spectra are detectable over time (Figure S29h), very much in contrast to $[Ru(bpy)_3]^{2+}$ and *fac*-$[Ir(ppy)_3]$ (Figure S29b/e).

The astonishing photorobustness of $[Co(L^{CNC})_2](PF_6)$ could have its origin in the fact that the rigid tridentate L^{CNC} ligand provides a nearly geometry-optimized coordination environment (Figure 2a) and simultaneously ensures a particularly tight binding of the metal trication through two carbenes and one anionic amido donor atom. In this particular binding situation, the extent of metal−ligand bond covalence

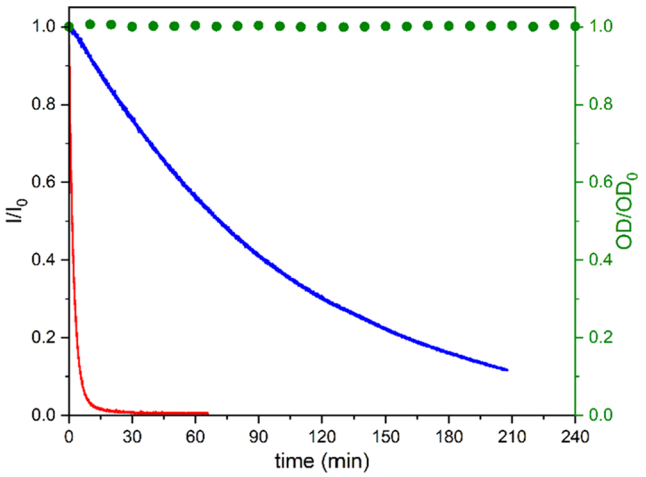

Figure 9. Comparative photostability studies of $[Co(L^{CNC})_2](PF_6)$, $[Ru(bpy)_3](PF_6)_2$, and *fac*-$[Ir(ppy)_3]$ in deaerated acetonitrile at 22 °C. Solutions with identical optical densities at 447 nm were irradiated with a continuous-wave laser providing an output power of 1.1 W at that wavelength. Red and blue traces: normalized photoluminescence intensities of $[Ru(bpy)_3](PF_6)_2$ at 620 nm and *fac*-$[Ir(ppy)_3]$ at 525 nm, respectively. Green circles: normalized absorbance of $[Co(L^{CNC})_2](PF_6)$ at 430 nm; UV−vis spectra recorded in time intervals of 10 min. UV−vis absorption spectra of all compounds before and after irradiation of all three compounds are shown in the Supporting Information (Figure S29).

should be substantially higher than in $[Ru(bpy)_3]^{2+}$, as well as in many other d^6 metal complexes, and it seems possible that this contributes to the photostability of $[Co(L^{CNC})_2](PF_6)$. Another key contributor is certainly the comparatively short excited-state lifetime of $[Co(L^{CNC})_2]^+$ (1.2 ns) in comparison to $[Ru(bpy)_3]^{2+}$ (830 ns)[161] and *fac*-$[Ir(ppy)_3]$ (1.9 μs),[162] which limits the probability for deleterious side reactions from the photoactive excited state.[129] This principle plays a key role for OLED triplet emitters, for which one typically targets high radiative excited-state decay rates to maximize the emission output and to minimize photodecomposition.[48,50,56,163,164]

Recently, a tris(diisocyanide)molybdenum(0) complex already showed good long-term photostability under high-power red (laser) irradiation at 635 nm,[165] and thus, the photorobustness of $[Co(L^{CNC})_2](PF_6)$ represents further evidence that d^6 complexes of earth-abundant transition metals can in fact be remarkably photostable.

CONCLUSIONS

Photoactive MLCT excited states are currently intensively investigated for the entire $3d^6$ series from chromium(0)[166−168] to manganese(I)[168,169] and iron(II),[36,55−57,74−87,90−95,168,169] whereas cobalt(III) complexes seem underexplored in this regard.[36,37] The comparatively high oxidation state of cobalt(III) usually favors low-lying LMCT excited states[89,104] and further can induce sufficiently strong ligand fields for the lowest MC state to become photoactive.[88,98,99] Regarding the photophysics of cobalt(III) compounds, the two main conceptual novelties of $[Co(L^{CNC})_2](PF_6)$ are (1) the fact that its energetically lowest-lying excited state has substantial MLCT character and (2) the observation that this excited state decays to the electronic ground state without a noticeable population of any MC state. These findings are in strong contrast to the vast majority of iron(II) complexes, in which lower-lying (and longer-lived) MC states typically deactivate

https://doi.org/10.1021/jacs.2c02592
J. Am. Chem. Soc. 2022, 144, 9859−9873

the MLCT state very rapidly and efficiently.[36,55−57,74−87,90−95,168,169] Controlling such excited-state decay paths is a key challenge in the first-row transition-metal complexes with d^6 or d^8 configurations, for which obtaining long-lived MLCT states is inherently more difficult than for copper(I) compounds with their filled $3d^{10}$ subshell.[44] If an MC state is involved in the excited-state relaxation pathway of $[Co(L^{CNC})_2]^+$ (e.g., by thermal population from the MLCT/ILCT manifold, as illustrated in Figure 7b), then the respective MC state would have to be very short-lived. In this case, the MC population could escape detection because the MC state decays faster than it is formed. This scenario could potentially explain the lack of photoluminescence in $[Co(L^{CNC})_2](PF_6)$. In addition to its substantial MLCT character, the photoactive excited state of $[Co(L^{CNC})_2](PF_6)$ has an intraligand contribution, making its overall composition qualitatively similar to that of the lowest excited state in many cyclometalated iridium(III) compounds.[4,12,13,20,170] Based on DFT calculations, the MLCT character of the photoactive excited state of $[Co(L^{CNC})_2]^+$ is limited (on the order of 10%). However, the cyclic voltammetry, spectro-electrochemical, and transient UV−vis absorption data point to much stronger metal involvement (Supporting Information Page S30). In particular, the comparison of picosecond transient absorption data with spectro-electrochemical data monitoring metal oxidation and ligand reduction (Figure 5) are much in line with substantial MLCT character. Furthermore, femtosecond transient absorption data (Figure 6) in comparison with spectro-electrochemical experiments (Figure S19) reveal noticeable differences between (predominant) MLCT and ILCT spectral signatures.

Except for its surprising photostability, the photophysical and photochemical behavior of $[Co(L^{CNC})_2](PF_6)$ is largely the anticipated result of careful ligand design. In this context, our study provides some insights (or at least hints) that seem relevant far beyond cobalt(III) complexes and which could affect a much broader range of transition-metal compounds. Recent investigations of photoactive first-row transition-metal complexes set much emphasis on the importance of ligand field strength (usually captured by the ligand field parameter 10 Dq), for which the σ-donor and π-acceptor properties of the ligands were optimized.[36,57,58,77,81,110,111,171,172] However, in addition to the ligand field strength, the metal−ligand bond covalence determines the energy of MC states (typically quantified by the so-called Racah B parameter), yet the importance of covalence could have been underestimated so far in the design of new photoactive transition-metal compounds.[96,118,173] The cobalt(III)−amido N(2p) bond in $[Co(L^{CNC})_2](PF_6)$ has substantial covalent character owing to the π-donor properties of the anionic carbazolate. This situation, in combination with the strong σ-donor properties of the four NHC units, is of key importance to obtain sufficient electron density at the metal center for a state with substantial MLCT character to become the lowest excited state. Furthermore, a high extent of metal−ligand bond covalence can contribute to a favorably high ratio between 10 Dq and B, leading to the scenario in which the MLCT state is not efficiently depopulated by lower-lying MC states as a result of their shift to very high energies. Our recent investigation of a chromium(III) complex with a mixed carbazolate-polypyridine ligand provided a remarkably low Racah B parameter,[118] which supports our speculation concerning the favorable 10 Dq/B ratio in $[Co(L^{CNC})_2](PF_6)$.

Computational and experimental work by other investigators already emphasized the importance of π-donation,[78,96,123,127,174] which is however often intuitively associated with a weakening of the ligand field strength.[92] We speculate that for this reason, π-donor ligands did so far not receive the amount of attention they would perhaps deserve for the design of new photoactive transition-metal compounds. Furthermore, it seems that metal−ligand bond covalence might be a somewhat underappreciated design factor in comparison to the more frequently considered strategies of establishing strong ligand fields, structural rigidity, and coordination geometry optimization.[37]

■ ASSOCIATED CONTENT

Supporting Information

The Supporting Information is available free of charge at https://pubs.acs.org/doi/10.1021/jacs.2c02592.

General procedures and equipment details, synthesis and characterization of ligand precursor and organometallic complexes, EPR data, X-ray data, NMR and HR-ESI mass spectra, cyclic voltammograms and spectro-electrochemistry data, photophysical data, and TD-DFT data (PDF)

Accession Codes

CCDC 2155721−2155722 contain the supplementary crystallographic data for this paper. These data can be obtained free of charge via www.ccdc.cam.ac.uk/data_request/cif, or by emailing data_request@ccdc.cam.ac.uk, or by contacting The Cambridge Crystallographic Data Centre, 12 Union Road, Cambridge CB2 1EZ, UK; fax: +44 1223 336033.

■ AUTHOR INFORMATION

Corresponding Author

Oliver S. Wenger − *Department of Chemistry, University of Basel, 4056 Basel, Switzerland;* orcid.org/0000-0002-0739-0553; Email: oliver.wenger@unibas.ch

Authors

Narayan Sinha − *Department of Chemistry, University of Basel, 4056 Basel, Switzerland;* orcid.org/0000-0002-0406-5552

Björn Pfund − *Department of Chemistry, University of Basel, 4056 Basel, Switzerland*

Christina Wegeberg − *Department of Chemistry, University of Basel, 4056 Basel, Switzerland;* orcid.org/0000-0002-6034-453X

Alessandro Prescimone − *Department of Chemistry, University of Basel, 4058 Basel, Switzerland;* orcid.org/0000-0002-3631-5210

Complete contact information is available at: https://pubs.acs.org/10.1021/jacs.2c02592

Notes

The authors declare no competing financial interest.

■ ACKNOWLEDGMENTS

This work was funded by the Swiss National Science Foundation through grant nos. 200021_178760 and 206021_157687 and the NCCR Molecular Systems Engineering. B.P. acknowledges a Ph. D. grant (number 14583224) by

the National Research Fund, Luxembourg. C.W. thanks the Independent Research Fund Denmark for an international postdoctoral grant (9059-00003B).

REFERENCES

(1) Costa, R. D.; Ortí, E.; Bolink, H. J.; Monti, F.; Accorsi, G.; Armaroli, N. Luminescent ionic transition-metal complexes for light-emitting electrochemical cells. *Angew. Chem., Int. Ed.* **2012**, *51*, 8178−8211.

(2) Henwood, A. F.; Zysman-Colman, E. Luminescent Iridium Complexes Used in Light-Emitting Electrochemical Cells (LEECs). *Top. Curr. Chem.* **2016**, *374*, 36.

(3) Krämer, J.; Kang, R.; Grimm, L. M.; De Cola, L.; Picchetti, P.; Biedermann, F. Molecular Probes, Chemosensors, and Nanosensors for Optical Detection of Biorelevant Molecules and Ions in Aqueous Media and Biofluids. *Chem. Rev.* **2022**, *122*, 3459−3636.

(4) Bevernaegie, R.; Wehlin, S. A. M.; Elias, B.; Troian-Gautier, L. A Roadmap Towards Visible Light Mediated Electron Transfer Chemistry with Iridium(III) Complexes. *ChemPhotoChem* **2021**, *5*, 217−234.

(5) Shon, J.-H.; Kim, D.; Rathnayake, M. D.; Sittel, S.; Weaver, J.; Teets, T. S. Photoredox catalysis on unactivated substrates with strongly reducing iridium photosensitizers. *Chem. Sci.* **2021**, *12*, 4069−4078.

(6) Welin, E. R.; Le, C.; Arias-Rotondo, D. M.; McCusker, J. K.; MacMillan, D. W. C. Photosensitized, energy transfer-mediated organometallic catalysis through electronically excited nickel(II). *Science* **2017**, *355*, 380−385.

(7) Arias-Rotondo, D. M.; McCusker, J. K. The photophysics of photoredox catalysis: a roadmap for catalyst design. *Chem. Soc. Rev.* **2016**, *45*, 5803−5820.

(8) Huang, J.; Gallucci, J. C.; Turro, C. Panchromatic dirhodium photocatalysts for dihydrogen generation with red light. *Chem. Sci.* **2020**, *11*, 9775−9783.

(9) Yang, M.; Yarnell, J. E.; El Roz, K.; Castellano, F. N. A Robust Visible-Light-Harvesting Cyclometalated Ir(III) Diimine Sensitizer for Homogeneous Photocatalytic Hydrogen Production. *ACS Appl. Energy Mater.* **2020**, *3*, 1842−1853.

(10) Singh-Rachford, T. N.; Castellano, F. N. Photon upconversion based on sensitized triplet−triplet annihilation. *Coord. Chem. Rev.* **2010**, *254*, 2560−2573.

(11) Bharmoria, P.; Bildirir, H.; Moth-Poulsen, K. Triplet-triplet annihilation based near infrared to visible molecular photon upconversion. *Chem. Soc. Rev.* **2020**, *49*, 6529−6554.

(12) Mills, I. N.; Porras, J. A.; Bernhard, S. Judicious Design of Cationic, Cyclometalated Ir(III) Complexes for Photochemical Energy Conversion and Optoelectronics. *Acc. Chem. Res.* **2018**, *51*, 352−364.

(13) Bevernaegie, R.; Wehlin, S. A. M.; Piechota, E. J.; Abraham, M.; Philouze, C.; Meyer, G. J.; Elias, B.; Troian-Gautier, L. Improved Visible Light Absorption of Potent Iridium(III) Photo-oxidants for Excited-State Electron Transfer Chemistry. *J. Am. Chem. Soc.* **2020**, *142*, 2732−2737.

(14) Heinemann, F.; Karges, J.; Gasser, G. Critical Overview of the Use of Ru(II) Polypyridyl Complexes as Photosensitizers in One-Photon and Two-Photon Photodynamic Therapy. *Acc. Chem. Res.* **2017**, *50*, 2727−2736.

(15) Swords, W. B.; Meyer, G. J.; Hammarström, L. Excited-state proton-coupled electron transfer within ion pairs. *Chem. Sci.* **2020**, *11*, 3460−3473.

(16) Sayre, H.; Ripberger, H. H.; Odella, E.; Zieleniewska, A.; Heredia, D. A.; Rumbles, G.; Scholes, G. D.; Moore, T. A.; Moore, A. L.; Knowles, R. R. PCET-Based Ligand Limits Charge Recombination with an Ir(III) Photoredox Catalyst. *J. Am. Chem. Soc.* **2021**, *143*, 13034−13043.

(17) Soupart, A.; Alary, F.; Heully, J.-L.; Elliott, P. I. P.; Dixon, I. M. Recent progress in ligand photorelease reaction mechanisms: Theoretical insights focusing on Ru(II) ^{3}MC states. *Coord. Chem. Rev.* **2020**, *408*, 213184.

(18) Proppe, A. H.; Li, Y. C.; Aspuru-Guzik, A.; Berlinguette, C. P.; Chang, C. J.; Cogdell, R.; Doyle, A. G.; Flick, J.; Gabor, N. M.; van Grondelle, R.; Hammes-Schiffer, S.; Jaffer, S. A.; Kelley, S. O.; Leclerc, M.; Leo, K.; Mallouk, T. E.; Narang, P.; Schlau-Cohen, G. S.; Scholes, G. D.; Vojvodic, A.; Yam, V. W.-W.; Yang, J. Y.; Sargent, E. H. Bioinspiration in light harvesting and catalysis. *Nat. Rev. Mater.* **2020**, *5*, 828−846.

(19) Shon, J.-H.; Teets, T. S. Molecular Photosensitizers in Energy Research and Catalysis: Design Principles and Recent Developments. *ACS Energy Lett.* **2019**, *4*, 558−566.

(20) DiLuzio, S.; Connell, T. U.; Mdluli, V.; Kowalewski, J. F.; Bernhard, S. Understanding Ir(III) Photocatalyst Structure-Activity Relationships: A Highly Parallelized Study of Light-Driven Metal Reduction Processes. *J. Am. Chem. Soc.* **2022**, *144*, 1431−1444.

(21) Wei, F.; Lai, S.-L.; Zhao, S.; Ng, M.; Chan, M.-Y.; Yam, V. W.-W.; Wong, K. M.-C. Ligand Mediated Luminescence Enhancement in Cyclometalated Rhodium(III) Complexes and Their Applications in Efficient Organic Light-Emitting Devices. *J. Am. Chem. Soc.* **2019**, *141*, 12863−12871.

(22) Chan, K.-T.; Lam, T. L.; Yu, D.; Du, L.; Phillips, D. L.; Kwong, C. L.; Tong, G. S. M.; Cheng, G.; Che, C. M. Strongly Luminescent Tungsten Emitters with Emission Quantum Yields of up to 84 %: TADF and High-Efficiency Molecular Tungsten OLEDs. *Angew. Chem., Int. Ed.* **2019**, *58*, 14896−14900.

(23) Connell, T. U.; Fraser, C. L.; Czyz, M. L.; Smith, Z. M.; Hayne, D. J.; Doeven, E. H.; Agugiaro, J.; Wilson, D. J. D.; Adcock, J. L.; Scully, A. D.; Gómez, D. E.; Barnett, N. W.; Polyzos, A.; Francis, P. S. The Tandem Photoredox Catalysis Mechanism of $[Ir(ppy)_2(dtb\text{-}bpy)]^+$ Enabling Access to Energy Demanding Organic Substrates. *J. Am. Chem. Soc.* **2019**, *141*, 17646−17658.

(24) Maurer, A. B.; Meyer, G. J. Stark Spectroscopic Evidence that a Spin Change Accompanies Light Absorption in Transition Metal Polypyridyl Complexes. *J. Am. Chem. Soc.* **2020**, *142*, 6847−6851.

(25) Strieth-Kalthoff, F.; Glorius, F. Triplet Energy Transfer Photocatalysis: Unlocking the Next Level. *Chem* **2020**, *6*, 1888−1903.

(26) Whittemore, T. J.; Xue, C.; Huang, J.; Gallucci, J. C.; Turro, C. Single-chromophore single-molecule photocatalyst for the production of dihydrogen using low-energy light. *Nat. Chem.* **2020**, *12*, 180−185.

(27) Coles, M. S.; Quach, G.; Beves, J. E.; Moore, E. G. A Photophysical Study of Sensitization-Initiated Electron Transfer: Insights into the Mechanism of Photoredox Activity. *Angew. Chem., Int. Ed.* **2020**, *59*, 9522−9526.

(28) Ranieri, A. M.; Burt, L. K.; Stagni, S.; Zacchini, S.; Skelton, B. W.; Ogden, M. I.; Bissember, A. C.; Massi, M. Anionic Cyclometalated Platinum(II) Tetrazolato Complexes as Viable Photoredox Catalysts. *Organometallics* **2019**, *38*, 1108−1117.

(29) Pander, P.; Daniels, R.; Zaytsev, A. V.; Horn, A.; Sil, A.; Penfold, T. J.; Williams, J. A. G.; Kozhevnikov, V. N.; Dias, F. B. Exceptionally fast radiative decay of a dinuclear platinum complex through thermally activated delayed fluorescence. *Chem. Sci.* **2021**, *12*, 6172−6180.

(30) Li, B.; Li, Y.; Chan, M. H.-Y.; Yam, V. W.-W. Phosphorescent Cyclometalated Platinum(II) Enantiomers with Circularly Polarized Luminescence Properties and Their Assembly Behaviors. *J. Am. Chem. Soc.* **2021**, *143*, 21676−21684.

(31) Amemori, S.; Sasaki, Y.; Yanai, N.; Kimizuka, N. Near-Infrared-to-Visible Photon Upconversion Sensitized by a Metal Complex with Spin-Forbidden yet Strong S_0-T_1 Absorption. *J. Am. Chem. Soc.* **2016**, *138*, 8702−8705.

(32) Ravetz, B. D.; Tay, N. E. S.; Joe, C. L.; Sezen-Edmonds, M.; Schmidt, M. A.; Tan, Y.; Janey, J. M.; Eastgate, M. D.; Rovis, T. Development of a Platform for Near-Infrared Photoredox Catalysis. *ACS Cent. Sci.* **2020**, *6*, 2053−2059.

(33) Schmid, L.; Glaser, F.; Schaer, R.; Wenger, O. S. High Triplet Energy Iridium(III) Isocyanoborato Complex for Photochemical Upconversion, Photoredox and Energy Transfer Catalysis. *J. Am. Chem. Soc.* **2022**, *144*, 963−976.

https://doi.org/10.1021/jacs.2c02592
J. Am. Chem. Soc. 2022, 144, 9859−9873

(34) Huang, X.; Meggers, E. Asymmetric Photocatalysis with Bis-cyclometalated Rhodium Complexes. *Acc. Chem. Res.* **2019**, *52*, 833−847.
(35) Sutton, J. J.; Preston, D.; Traber, P.; Steinmetzer, J.; Wu, X.; Kayal, S.; Sun, X.-Z.; Crowley, J. D.; George, M. W.; Kupfer, S.; Gordon, K. C. Excited-State Switching in Rhenium(I) Bipyridyl Complexes with Donor-Donor and Donor-Acceptor Substituents. *J. Am. Chem. Soc.* **2021**, *143*, 9082−9093.
(36) Förster, C.; Heinze, K. Photophysics and Photochemistry with Earth-Abundant Metals - Fundamentals and Concepts. *Chem. Soc. Rev.* **2020**, *49*, 1057−1070.
(37) Wegeberg, C.; Wenger, O. S. Luminescent First-Row Transition Metal Complexes. *JACS Au* **2021**, *1*, 1860−1876.
(38) Hockin, B. M.; Li, C.; Robertson, N.; Zysman-Colman, E. Photoredox catalysts based on earth-abundant metal complexes. *Catal. Sci. Technol.* **2019**, *9*, 889−915.
(39) Li, Q. Y.; Gockel, S. N.; Lutovsky, G. A.; DeGlopper, K. S.; Baldwin, N. J.; Bundesmann, M. W.; Tucker, J. W.; Bagley, S. W.; Yoon, T. P. Decarboxylative cross-nucleophile coupling via ligand-to-metal charge transfer photoexcitation of Cu(II) carboxylates. *Nat. Chem.* **2022**, *14*, 94−99.
(40) Paulus, B. C.; Adelman, S. L.; Jamula, L. L.; McCusker, J. K. Leveraging excited-state coherence for synthetic control of ultrafast dynamics. *Nature* **2020**, *582*, 214−218.
(41) Chábera, P.; Liu, Y.; Prakash, O.; Thyrhaug, E.; Nahhas, A. E.; Honarfar, A.; Essen, S.; Fredin, L. A.; Harlang, T. C.; Kjaer, K. S.; Handrup, K.; Ericson, F.; Tatsuno, H.; Morgan, K.; Schnadt, J.; Haggstrom, L.; Ericsson, T.; Sobkowiak, A.; Lidin, S.; Huang, P.; Styring, S.; Uhlig, J.; Bendix, J.; Lomoth, R.; Sundström, V.; Persson, P.; Wärnmark, K. A low-spin Fe(III) complex with 100-ps ligand-to-metal charge transfer photoluminescence. *Nature* **2017**, *543*, 695−699.
(42) Kainz, Q. M.; Matier, C. D.; Bartoszewicz, A.; Zultanski, S. L.; Peters, J. C.; Fu, G. C. Asymmetric copper-catalyzed C-N cross-couplings induced by visible light. *Science* **2016**, *351*, 681−684.
(43) Gygi, D.; Gonzalez, M. I.; Hwang, S. J.; Xia, K. T.; Qin, Y.; Johnson, E. J.; Gygi, F.; Chen, Y.-S.; Nocera, D. G. Capturing the Complete Reaction Profile of a C-H Bond Activation. *J. Am. Chem. Soc.* **2021**, *143*, 6060−6064.
(44) McCusker, J. K. Electronic structure in the transition metal block and its implications for light harvesting. *Science* **2019**, *363*, 484−488.
(45) Lazorski, M. S.; Castellano, F. N. Advances in the light conversion properties of Cu(I)-based photosensitizers. *Polyhedron* **2014**, *82*, 57−70.
(46) Hossain, A.; Bhattacharyya, A.; Reiser, O. Copper's rapid ascent in visible-light photoredox catalysis. *Science* **2019**, *364*, No. eaav9713.
(47) Minozzi, C.; Caron, A.; Grenier-Petel, J.-C.; Santandrea, J.; Collins, S. K. Heteroleptic Copper(I)-Based Complexes for Photocatalysis: Combinatorial Assembly, Discovery, and Optimization. *Angew. Chem., Int. Ed.* **2018**, *57*, 5477−5481.
(48) Hamze, R.; Peltier, J. L.; Sylvinson, D.; Jung, M.; Cardenas, J.; Haiges, R.; Soleilhavoup, M.; Jazzar, R.; Djurovich, P. I.; Bertrand, G.; Thompson, M. E. Eliminating nonradiative decay in Cu(I) emitters: >99% quantum efficiency and microsecond lifetime. *Science* **2019**, *363*, 601−606.
(49) Di, D.; Romanov, A. S.; Yang, L.; Richter, J. M.; Rivett, J. P. H.; Jones, S.; Thomas, T. H.; Jalebi, M. A.; Friend, R. H.; Linnolahti, M.; Bochmann, M.; Credgington, D. High-performance light-emitting diodes based on carbene-metal-amides. *Science* **2017**, *356*, 159−163.
(50) Gernert, M.; Balles-Wolf, L.; Kerner, F.; Müller, U.; Schmiedel, A.; Holzapfel, M.; Marian, C. M.; Pflaum, J.; Lambert, C.; Steffen, A. Cyclic (Amino)(aryl)carbenes Enter the Field of Chromophore Ligands: Expanded pi System Leads to Unusually Deep Red Emitting Cu(I) Compounds. *J. Am. Chem. Soc.* **2020**, *142*, 8897−8909.
(51) Shaw, G. B.; Grant, C. D.; Shirota, H.; Castner, E. W., Jr.; Meyer, G. J.; Chen, L. X. Ultrafast Structural Rearrangements in the MLCT Excited State for Copper(I) bis-Phenanthrolines in Solution. *J. Am. Chem. Soc.* **2007**, *129*, 2147−2160.
(52) Housecroft, C. E.; Constable, E. C. The emergence of copper(I)-based dye sensitized solar cells. *Chem. Soc. Rev.* **2015**, *44*, 8386−8398.
(53) Khnayzer, R. S.; McCusker, C. E.; Olaiya, B. S.; Castellano, F. N. Robust cuprous phenanthroline sensitizer for solar hydrogen photocatalysis. *J. Am. Chem. Soc.* **2013**, *135*, 14068−14070.
(54) Dietrich-Buchecker, C. O.; Marnot, P. A.; Sauvage, J.-P.; Kirchhoff, J. R.; McMillin, D. R. Bis(2,9-diphenyl-1,10-phenanthroline)copper(1) : a Copper Complex with a Long-lived Charge-transfer Excited State. *J. Chem. Soc., Chem. Commun.* **1983**, 513−515.
(55) Cuttell, D. G.; Kuang, S.-M.; Fanwick, P. E.; McMillin, D. R.; Walton, R. A. Simple Cu(I) Complexes with Unprecedented Excited-State Lifetimes. *J. Am. Chem. Soc.* **2002**, *124*, 6−7.
(56) Czerwieniec, R.; Leitl, M. J.; Homeier, H. H. H.; Yersin, H. Cu(I) complexes−Thermally activated delayed fluorescence. Photophysical approach and material design. *Coord. Chem. Rev.* **2016**, *325*, 2−28.
(57) Otto, S.; Dorn, M.; Förster, C.; Bauer, M.; Seitz, M.; Heinze, K. Understanding and Exploiting Long-Lived Near-Infrared Emission of a Molecular Ruby. *Coord. Chem. Rev.* **2018**, *359*, 102−111.
(58) Reichenauer, F.; Wang, C.; Förster, C.; Boden, P.; Ugur, N.; Báez-Cruz, R.; Kalmbach, J.; Carrella, L. M.; Rentschler, E.; Ramanan, C.; Niedner-Schatteburg, G.; Gerhards, M.; Seitz, M.; Resch-Genger, U.; Heinze, K. Strongly Red-Emissive Molecular Ruby $[Cr(bpmp)_2]^{3+}$ Surpasses $[Ru(bpy)_3]^{2+}$. *J. Am. Chem. Soc.* **2021**, *143*, 11843−11855.
(59) Jiménez, J.-R.; Doistau, B.; Cruz, C. M.; Besnard, C.; Cuerva, J. M.; Campaña, A. G.; Piguet, C. Chiral Molecular Ruby $[Cr(dqp)_2]^{3+}$ with Long-Lived Circularly Polarized Luminescence. *J. Am. Chem. Soc.* **2019**, *141*, 13244−13252.
(60) Treiling, S.; Wang, C.; Förster, C.; Reichenauer, F.; Kalmbach, J.; Boden, P.; Harris, J. P.; Carrella, L. M.; Rentschler, E.; Resch-Genger, U.; Reber, C.; Seitz, M.; Gerhards, M.; Heinze, K. Luminescence and Light-Driven Energy and Electron Transfer from an Exceptionally Long-Lived Excited State of a Non-Innocent Chromium(III) Complex. *Angew. Chem., Int. Ed.* **2019**, *58*, 18075−18085.
(61) Wang, C.; Otto, S.; Dorn, M.; Kreidt, E.; Lebon, J.; Sršan, L.; Di Martino-Fumo, P.; Gerhards, M.; Resch-Genger, U.; Seitz, M.; Heinze, K. Deuterated Molecular Ruby with Record Luminescence Quantum Yield. *Angew. Chem., Int. Ed.* **2018**, *57*, 1112−1116.
(62) Jiménez, J. R.; Poncet, M.; Míguez-Lago, S.; Grass, S.; Lacour, J.; Besnard, C.; Cuerva, J. M.; Campaña, A. G.; Piguet, C. Bright Long-Lived Circularly Polarized Luminescence in Chiral Chromium(III) Complexes. *Angew. Chem., Int. Ed.* **2021**, *60*, 10095−10102.
(63) Wong, Y.-S.; Tang, M.-C.; Ng, M.; Yam, V. W.-W. Toward the Design of Phosphorescent Emitters of Cyclometalated Earth-Abundant Nickel(II) and Their Supramolecular Study. *J. Am. Chem. Soc.* **2020**, *142*, 7638−7646.
(64) Ting, S. I.; Garakyaraghi, S.; Taliaferro, C. M.; Shields, B. J.; Scholes, G. D.; Castellano, F. N.; Doyle, A. G. ^{3}d-d Excited States of Ni(II) Complexes Relevant to Photoredox Catalysis: Spectroscopic Identification and Mechanistic Implications. *J. Am. Chem. Soc.* **2020**, *142*, 5800−5810.
(65) Wenger, O. S. Photoactive Nickel Complexes in Cross-Coupling Catalysis. *Chem.—Eur. J.* **2021**, *27*, 2270−2278.
(66) Shields, B. J.; Kudisch, B.; Scholes, G. D.; Doyle, A. G. Long-Lived Charge-Transfer States of Nickel(II) Aryl Halide Complexes Facilitate Bimolecular Photoinduced Electron Transfer. *J. Am. Chem. Soc.* **2018**, *140*, 3035−3039.
(67) Yam, V. W.-W.; Chan, A. K.-W.; Hong, E. Y.-H. Charge-transfer processes in metal complexes enable luminescence and memory functions. *Nat. Rev. Chem* **2020**, *4*, 528−541.
(68) Balzani, V.; Ceroni, P.; Credi, A.; Venturi, M. Ruthenium tris(bipyridine) complexes: Interchange between photons and electrons in molecular-scale devices and machines. *Coord. Chem. Rev.* **2021**, *433*, 213758.
(69) Malmberg, R.; Venkatesan, K. Conceptual advances in the preparation and excited-state properties of neutral luminescent (C^N)

https://doi.org/10.1021/jacs.2c02592
J. Am. Chem. Soc. 2022, 144, 9859−9873

and (C^C*) monocyclometalated gold(III) complexes. *Coord. Chem. Rev.* **2021**, *449*, 214182.
(70) Cordero, M. A. A.; Boden, P. J.; Rentschler, M.; Di Martino-Fumo, P.; Frey, W.; Yang, Y.; Gerhards, M.; Karnahl, M.; Lochbrunner, S.; Tschierlei, S. Comprehensive Picture of the Excited State Dynamics of Cu(I)- and Ru(II)-Based Photosensitizers with Long-Lived Triplet States. *Inorg. Chem.* **2022**, *61*, 214−226.
(71) Zedler, L.; Mengele, A. K.; Ziems, K. M.; Zhang, Y.; Wächtler, M.; Gräfe, S.; Pascher, T.; Rau, S.; Kupfer, S.; Dietzek, B. Unraveling the Light-Activated Reaction Mechanism in a Catalytically Competent Key Intermediate of a Multifunctional Molecular Catalyst for Artificial Photosynthesis. *Angew. Chem., Int. Ed.* **2019**, *58*, 13140−13148.
(72) Lo, K. K.-W. Luminescent Rhenium(I) and Iridium(III) Polypyridine Complexes as Biological Probes, Imaging Reagents, and Photocytotoxic Agents. *Acc. Chem. Res.* **2015**, *48*, 2985−2995.
(73) Juris, A.; Balzani, V.; Barigelletti, F.; Campagna, S.; Belser, P.; Von Zelewsky, A. Ru(II) Polypyridine Complexes: Photophysics, Photochemistry, Electrochemistry, and Chemi-Luminescence. *Coord. Chem. Rev.* **1988**, *84*, 85−277.
(74) Auböck, G.; Chergui, M. Sub-50-fs photoinduced spin crossover in $[Fe(bpy)_3]^{2+}$. *Nat. Chem.* **2015**, *7*, 629−633.
(75) Carey, M. C.; Adelman, S. L.; McCusker, J. K. Insights into the excited state dynamics of Fe(II) polypyridyl complexes from variable-temperature ultrafast spectroscopy. *Chem. Sci.* **2019**, *10*, 134−144.
(76) Zhang, K.; Ash, R.; Girolami, G. S.; Vura-Weis, J. Tracking the Metal-Centered Triplet in Photoinduced Spin Crossover of Fe-$(phen)_3^{2+}$ with Tabletop Femtosecond M-Edge X-ray Absorption Near-Edge Structure Spectroscopy. *J. Am. Chem. Soc.* **2019**, *141*, 17180−17188.
(77) Chábera, P.; Kjaer, K. S.; Prakash, O.; Honarfar, A.; Liu, Y.; Fredin, L. A.; Harlang, T. C. B.; Lidin, S.; Uhlig, J.; Sundstrom, V.; Lomoth, R.; Persson, P.; Wärnmark, K. Fe^{II} Hexa N-Heterocyclic Carbene Complex with a 528 ps Metal-to-Ligand Charge-Transfer Excited-State Lifetime. *J. Phys. Chem. Lett.* **2018**, *9*, 459−463.
(78) Braun, J. D.; Lozada, I. B.; Kolodziej, C.; Burda, C.; Newman, K. M. E.; van Lierop, J.; Davis, R. L.; Herbert, D. E. Iron(II) Coordination Complexes with Panchromatic Absorption and Nanosecond Charge-Transfer Excited State Lifetimes. *Nat. Chem.* **2019**, *11*, 1144−1150.
(79) Fatur, S. M.; Shepard, S. G.; Higgins, R. F.; Shores, M. P.; Damrauer, N. H. A Synthetically Tunable System To Control MLCT Excited-State Lifetimes and Spin States in Iron(II) Polypyridines. *J. Am. Chem. Soc.* **2017**, *139*, 4493−4505.
(80) Shepard, S. G.; Fatur, S. M.; Rappé, A. K.; Damrauer, N. H. Highly Strained Iron(II) Polypyridines: Exploiting the Quintet Manifold To Extend the Lifetime of MLCT Excited States. *J. Am. Chem. Soc.* **2016**, *138*, 2949−2952.
(81) Duchanois, T.; Liu, L.; Pastore, M.; Monari, A.; Cebrián, C.; Trolez, Y.; Darari, M.; Magra, K.; Francés-Monerris, A.; Domenichini, E.; Beley, M.; Assfeld, X.; Haacke, S.; Gros, P. NHC-Based Iron Sensitizers for DSSCs. *Inorganics* **2018**, *6*, 63.
(82) Reuter, T.; Kruse, A.; Schoch, R.; Lochbrunner, S.; Bauer, M.; Heinze, K. Higher MLCT lifetime of carbene iron(II) complexes by chelate ring expansion. *Chem. Commun.* **2021**, *57*, 7541−7544.
(83) Jiang, T.; Bai, Y.; Zhang, P.; Han, Q.; Mitzi, D. B.; Therien, M. J. Electronic structure and photophysics of a supermolecular iron complex having a long MLCT-state lifetime and panchromatic absorption. *Proc. Natl. Acad. Sci.* **2020**, *117*, 20430−20437.
(84) Woodhouse, M. D.; McCusker, J. K. Mechanistic Origin of Photoredox Catalysis Involving Iron(II) Polypyridyl Chromophores. *J. Am. Chem. Soc.* **2020**, *142*, 16229−16233.
(85) Gualandi, A.; Marchini, M.; Mengozzi, L.; Natali, M.; Lucarini, M.; Ceroni, P.; Cozzi, P. G. Organocatalytic Enantioselective Alkylation of Aldehydes with $[Fe(bpy)_3Br_2$ Catalyst and Visible Light. *ACS Catal.* **2015**, *5*, 5927−5931.
(86) Zhou, W. J.; Wu, X. D.; Miao, M.; Wang, Z. H.; Chen, L.; Shan, S. Y.; Cao, G. M.; Yu, D. G. Light Runs Across Iron Catalysts in Organic Transformations. *Chem.—Eur. J.* **2020**, *26*, 15052−15064.
(87) Leis, W.; Cordero, M. A.; Lochbrunner, S.; Schubert, H.; Berkefeld, A. A Photoreactive Iron(II) Complex Luminophore. *J. Am. Chem. Soc.* **2022**, *144*, 1169−1173.
(88) Kaufhold, S.; Rosemann, N. W.; Chábera, P.; Lindh, L.; Losada, I.; Uhlig, J.; Pascher, T.; Strand, D.; Wärnmark, K.; Yartsev, A.; Persson, P. Microsecond Photoluminescence and Photoreactivity of a Metal-Centered Excited State in a Hexacarbene-Co(III) Complex. *J. Am. Chem. Soc.* **2021**, *143*, 1307−1312.
(89) Pal, A. K.; Li, C.; Hanan, G. S.; Zysman-Colman, E. Blue-Emissive Cobalt(III) Complexes and Their Use in the Photocatalytic Trifluoromethylation of Polycyclic Aromatic Hydrocarbons. *Angew. Chem., Int. Ed.* **2018**, *57*, 8027−8031.
(90) Dierks, P.; Päpcke, A.; Bokareva, O. S.; Altenburger, B.; Reuter, T.; Heinze, K.; Kühn, O.; Lochbrunner, S.; Bauer, M. Ground- and Excited-State Properties of Iron(II) Complexes Linked to Organic Chromophores. *Inorg. Chem.* **2020**, *59*, 14746−14761.
(91) Cammarata, M.; Zerdane, S.; Balducci, L.; Azzolina, G.; Mazerat, S.; Exertier, C.; Trabuco, M.; Levantino, M.; Alonso-Mori, R.; Glownia, J. M.; Song, S.; Catala, L.; Mallah, T.; Matar, S. F.; Collet, E. Charge transfer driven by ultrafast spin transition in a CoFe Prussian blue analogue. *Nat. Chem.* **2021**, *13*, 10−14.
(92) Wenger, O. S. Is Iron the New Ruthenium? *Chem.—Eur. J.* **2019**, *25*, 6043−6052.
(93) Kurz, H.; Schötz, K.; Papadopoulos, I.; Heinemann, F. W.; Maid, H.; Guldi, D. M.; Köhler, A.; Hörner, G.; Weber, B. A Fluorescence-Detected Coordination-Induced Spin State Switch. *J. Am. Chem. Soc.* **2021**, *143*, 3466−3480.
(94) Dierks, P.; Vukadinovic, Y.; Bauer, M. Photoactive iron complexes: more sustainable, but still a challenge. *Inorg. Chem. Front.* **2022**, *9*, 206−220.
(95) Paulus, B. C.; Nielsen, K. C.; Tichnell, C. R.; Carey, M. C.; McCusker, J. K. A Modular Approach to Light Capture and Synthetic Tuning of the Excited-State Properties of Fe(II)-Based Chromophores. *J. Am. Chem. Soc.* **2021**, *143*, 8086−8098.
(96) Larsen, C. B.; Braun, J. D.; Lozada, I. B.; Kunnus, K.; Biasin, E.; Kolodziej, C.; Burda, C.; Cordones, A. A.; Gaffney, K. J.; Herbert, D. E. Reduction of Electron Repulsion in Highly Covalent Fe-Amido Complexes Counteracts the Impact of a Weak Ligand Field on Excited-State Ordering. *J. Am. Chem. Soc.* **2021**, *143*, 20645−20656.
(97) Hauser, A.; Reber, C. Spectroscopy and Chemical Bonding in Transition Metal Complexes. *Struct. Bond* **2016**, *172*, 291−312.
(98) Viaene, L.; D'Olieslager, J. Luminescence from and absorption by the $^3T_{1g}$ Level of the Hexacyanocobaltate(III) Ion. *Inorg. Chem.* **1987**, *26*, 960−962.
(99) Viaene, L.; D'Olieslager, J.; Ceulemans, A.; Vanquickenborne, L. G. Excited-State Spectroscopy of Hexacyanocobaltate(III). *J. Am. Chem. Soc.* **1979**, *101*, 1405−1409.
(100) Aydogan, A.; Bangle, R. E.; Cadranel, A.; Turlington, M. D.; Conroy, D. T.; Cauët, E.; Singleton, M. L.; Meyer, G. J.; Sampaio, R. N.; Elias, B.; Troian-Gautier, L. Accessing Photoredox Transformations with an Iron(III) Photosensitizer and Green Light. *J. Am. Chem. Soc.* **2021**, *143*, 15661−15673.
(101) Zhang, Y.; Lee, T. S.; Favale, J. M.; Leary, D. C.; Petersen, J. L.; Scholes, G. D.; Castellano, F. N.; Milsmann, C. Delayed fluorescence from a zirconium(IV) photosensitizer with ligand-to-metal charge-transfer excited states. *Nat. Chem.* **2020**, *12*, 345−352.
(102) Rosemann, N. W.; Chábera, P.; Prakash, O.; Kaufhold, S.; Wärnmark, K.; Yartsev, A.; Persson, P. Tracing the Full Bimolecular Photocycle of Iron(III)-Carbene Light Harvesters in Electron-Donating Solvents. *J. Am. Chem. Soc.* **2020**, *142*, 8565−8569.
(103) Kaul, N.; Lomoth, R. The Carbene Cannibal: Photoinduced Symmetry-Breaking Charge Separation in an Fe(III) N-Heterocyclic Carbene. *J. Am. Chem. Soc.* **2021**, *143*, 10816−10821.
(104) Wenger, O. S. A bright future for photosensitizers. *Nat. Chem.* **2020**, *12*, 323−324.
(105) Harris, J. P.; Reber, C.; Colmer, H. E.; Jackson, T. A.; Forshaw, A. P.; Smith, J. M.; Kinney, R. A.; Telser, J. Near-infrared $^2E_g \rightarrow {}^4A_{2g}$ and visible LMCT luminescence from a molecular bis-

https://doi.org/10.1021/jacs.2c02592
J. Am. Chem. Soc. 2022, 144, 9859−9873

(tris(carbene)borate) manganese(IV) complex. *Can. J. Chem.* **2017**, *95*, 547−552.
(106) Yang, M.; Sheykhi, S.; Zhang, Y.; Milsmann, C.; Castellano, F. N. Low power threshold photochemical upconversion using a zirconium(IV) LMCT photosensitizer. *Chem. Sci.* **2021**, *12*, 9069−9077.
(107) Kjær, K. S.; Kaul, N.; Prakash, O.; Chabera, P.; Rosemann, N. W.; Honarfar, A.; Gordivska, O.; Fredin, L. A.; Bergquist, K. E.; Haggstrom, L.; Ericsson, T.; Lindh, L.; Yartsev, A.; Styring, S.; Huang, P.; Uhlig, J.; Bendix, J.; Strand, D.; Sundstrom, V.; Persson, P.; Lomoth, R.; Wärnmark, K. Luminescence and reactivity of a charge-transfer excited iron complex with nanosecond lifetime. *Science* **2019**, *363*, 249−253.
(108) London, H. C.; Whittemore, T. J.; Gale, A. G.; McMillen, C. D.; Pritchett, D. Y.; Myers, A. R.; Thomas, H. D.; Shields, G. C.; Wagenknecht, P. S. Ligand-to-Metal Charge-Transfer Photophysics and Photochemistry of Emissive d^0 Titanocenes: A Spectroscopic and Computational Investigation. *Inorg. Chem.* **2021**, *60*, 14399−14409.
(109) Qiao, Y.; Schelter, E. J. Lanthanide Photocatalysis. *Acc. Chem. Res.* **2018**, *51*, 2926−2936.
(110) Jamula, L. L.; Brown, A. M.; Guo, D.; McCusker, J. K. Synthesis and characterization of a high-symmetry ferrous polypyridyl complex: approaching the $^5T_2/^3T_1$ crossing point for Fe(II). *Inorg. Chem.* **2014**, *53*, 15−17.
(111) Otto, S.; Grabolle, M.; Förster, C.; Kreitner, C.; Resch-Genger, U.; Heinze, K. $[Cr(ddpd)_2]^{3+}$: A Molecular, Water-Soluble, Highly NIR-Emissive Ruby Analogue. *Angew. Chem., Int. Ed.* **2015**, *54*, 11572−11576.
(112) Moser, M.; Wucher, B.; Kunz, D.; Rominger, F. 1,8-Bis(imidazolin-2-yliden-1-yl)carbazolide (bimca): A New CNC Pincer-Type Ligand with Strong Electron-Donating Properties. Facile Oxidative Addition of Methyl Iodide to Rh(bimca)(CO). *Organometallics* **2007**, *26*, 1024−1030.
(113) Seyboldt, A.; Wucher, B.; Alles, M.; Rominger, F.; Maichle-Mössmer, C.; Kunz, D. Synthesis and reactivity of an Ir(I) carbonyl complex bearing a carbazolide-bis(NHC) pincer ligand. *J. Organomet. Chem.* **2015**, *775*, 202−208.
(114) Jürgens, E.; Buys, K. N.; Schmidt, A.-T.; Furfari, S. K.; Cole, M. L.; Moser, M.; Rominger, F.; Kunz, D. Optimised synthesis of monoanionic bis(NHC)-pincer ligand precursors and their Li-complexes. *New J. Chem.* **2016**, *40*, 9160−9169.
(115) Seyboldt, A.; Wucher, B.; Hohnstein, S.; Eichele, K.; Rominger, F.; Törnroos, K. W.; Kunz, D. Evidence for the Formation of Anionic Zerovalent Group 10 Complexes as Highly Reactive Intermediates. *Organometallics* **2015**, *34*, 2717−2725.
(116) Liska, T.; Swetz, A.; Lai, P. N.; Zeller, M.; Teets, T. S.; Gray, T. G. Room-Temperature Phosphorescent Platinum(II) Alkynyls with Microsecond Lifetimes Bearing a Strong-Field Pincer Ligand. *Chem.—Eur. J.* **2020**, *26*, 8417−8425.
(117) Liska, T.; Li, M.; Cañada, L. M.; Yoon, S.; Teets, T. S.; Zeller, M.; Gray, T. G. Enhancing Charge Transfer in (BIMCA)Pt(II) Alkynyls through the Use of Substituted Boranes. *Organometallics* **2021**, *40*, 1555−1559.
(118) Sinha, N.; Jiménez, J. R.; Pfund, B.; Prescimone, A.; Piguet, C.; Wenger, O. S. A Near-Infrared-II Emissive Chromium(III) Complex. *Angew. Chem., Int. Ed.* **2021**, *60*, 23722−23728.
(119) Cahn, R. S.; Ingold, C.; Prelog, V. Specification of Molecular Chirality. *Angew. Chem., Int. Ed. Engl.* **1966**, *5*, 385−415.
(120) Dee, C.; Zinna, F.; Kitzmann, W. R.; Pescitelli, G.; Heinze, K.; Di Bari, L.; Seitz, M. Strong circularly polarized luminescence of an octahedral chromium(III) complex. *Chem. Commun.* **2019**, *55*, 13078−13081.
(121) Bauer, M.; Steube, J.; Päpcke, A.; Bokareva, O.; Reuter, T.; Demeshko, S.; Schoch, R.; Hohloch, S.; Meyer, F.; Heinze, K.; Kühn, O.; Lochbrunner, S. Janus-type dual emission of a Cyclometalated Iron(III) complex. *Res. Sq.* **2020**, DOI: 10.21203/rs.3.rs-64316/v1.
(122) Indumathy, R.; Weyhermüller, T.; Nair, B. U. Biimidazole containing cobalt(III) mixed ligand complexes: Crystal structure and photonuclease activity. *Dalton Trans.* **2010**, *39*, 2087−2097.
(123) Braun, J. D.; Lozada, I. B.; Herbert, D. E. In Pursuit of Panchromatic Absorption in Metal Coordination Complexes: Experimental Delineation of the HOMO Inversion Model Using Pseudo-Octahedral Complexes of Diarylamido Ligands. *Inorg. Chem.* **2020**, *59*, 17746−17757.
(124) Elgrishi, N.; Rountree, K. J.; McCarthy, B. D.; Rountree, E. S.; Eisenhart, T. T.; Dempsey, J. L. A Practical Beginner's Guide to Cyclic Voltammetry. *J. Chem. Educ.* **2017**, *95*, 197−206.
(125) Keilwerth, M.; Grunwald, L.; Mao, W.; Heinemann, F. W.; Sutter, J.; Bill, E.; Meyer, K. Ligand Tailoring Toward an Air-Stable Iron(V) Nitrido Complex. *J. Am. Chem. Soc.* **2021**, *143*, 1458−1465.
(126) Dodsworth, E. S.; Lever, A. B. P. Correlations between electrochemical potentials and optical charge transfer energies in ruthenium bipyridine derivatives. *Chem. Phys. Lett.* **1986**, *124*, 152−158.
(127) Mukherjee, S.; Torres, D. E.; Jakubikova, E. HOMO inversion as a strategy for improving the light-absorption properties of Fe(II) chromophores. *Chem. Sci.* **2017**, *8*, 8115−8126.
(128) Yoshimura, A.; Hoffman, M. Z.; Sun, H. An Evaluation of the Excited-State Absorption-Spectrum of $Ru(bpy)_3^{2+}$ in Aqueous and Acetonitrile Solutions. *J. Photochem. Photobiol., A* **1993**, *70*, 29−33.
(129) Schmid, L.; Kerzig, C.; Prescimone, A.; Wenger, O. S. Photostable Ruthenium(II) Isocyanoborato Luminophores and Their Use in Energy Transfer and Photoredox Catalysis. *JACS Au* **2021**, *1*, 819−832.
(130) Damrauer, N. H.; Cerullo, G.; Yeh, A.; Boussie, T. R.; Shank, C. V.; McCusker, J. K. Femtosecond Dynamics of Excited-State Evolution in $[Ru(bpy)_3]^{2+}$. *Science* **1997**, *275*, 54−57.
(131) Brown, A. M.; McCusker, C. E.; McCusker, J. K. Spectroelectrochemical identification of charge-transfer excited states in transition metal-based polypyridyl complexes. *Dalton Trans.* **2014**, *43*, 17635−17646.
(132) Parisien-Collette, S.; Hernandez-Perez, A. C.; Collins, S. K. Photochemical Synthesis of Carbazoles Using an $[Fe(phen)_3](NTf_2)_2/O_2$ Catalyst System: Catalysis toward Sustainability. *Org. Lett.* **2016**, *18*, 4994−4997.
(133) Ryland, E. S.; Zhang, K.; Vura-Weis, J. Sub-100 fs Intersystem Crossing to a Metal-Centered Triplet in Ni(II)OEP Observed with M-Edge XANES. *J. Phys. Chem. A* **2019**, *123*, 5214−5222.
(134) Phelan, B. T.; Mara, M. W.; Chen, L. X. Excited-state structural dynamics of nickel complexes probed by optical and X-ray transient absorption spectroscopies: insights and implications. *Chem. Commun.* **2021**, *57*, 11904−11921.
(135) Zhang, W.; Gaffney, K. J. Mechanistic Studies of Photo-induced Spin Crossover and Electron Transfer in Inorganic Complexes. *Acc. Chem. Res.* **2015**, *48*, 1140−1148.
(136) Kjær, K. S.; Van Driel, T. B.; Harlang, T. C. B.; Kunnus, K.; Biasin, E.; Ledbetter, K.; Hartsock, R. W.; Reinhard, M. E.; Koroidov, S.; Li, L.; Laursen, M. G.; Hansen, F. B.; Vester, P.; Christensen, M.; Haldrup, K.; Nielsen, M. M.; Dohn, A. O.; Papai, M. I.; Moller, K. B.; Chábera, P.; Liu, Y.; Tatsuno, H.; Timm, C.; Jarenmark, M.; Uhlig, J.; Sundström, V.; Wärnmark, K.; Persson, P.; Nemeth, Z.; Szemes, D. S.; Bajnoczi, E.; Vanko, G.; Alonso-Mori, R.; Glownia, J. M.; Nelson, S.; Sikorski, M.; Sokaras, D.; Canton, S. E.; Lemke, H. T.; Gaffney, K. J. Finding intersections between electronic excited state potential energy surfaces with simultaneous ultrafast X-ray scattering and spectroscopy. *Chem. Sci.* **2019**, *10*, 5749−5760.
(137) Gray, H. B.; Maverick, A. W. Solar Chemistry of Metal Complexes. *Science* **1981**, *214*, 1201−1205.
(138) Murray, P. R. D.; Cox, J. H.; Chiappini, N. D.; Roos, C. B.; McLoughlin, E. A.; Hejna, B. G.; Nguyen, S. T.; Ripberger, H. H.; Ganley, J. M.; Tsui, E.; Shin, N. Y.; Koronkiewicz, B.; Qiu, G.; Knowles, R. R. Photochemical and Electrochemical Applications of Proton-Coupled Electron Transfer in Organic Synthesis. *Chem. Rev.* **2022**, *122*, 2017−2291.
(139) Hammarström, L. Accumulative charge separation for solar fuels production: coupling light-induced single electron transfer to multielectron catalysis. *Acc. Chem. Res.* **2015**, *48*, 840−850.

(140) Amthor, S.; Knoll, S.; Heiland, M.; Zedler, L.; Li, C.; Nauroozi, D.; Tobaschus, W.; Mengele, A. K.; Anjass, M.; Schubert, U. S.; Dietzek-Ivanšić, B.; Rau, S.; Streb, C. A photosensitizer-polyoxometalate dyad that enables the decoupling of light and dark reactions for delayed on-demand solar hydrogen production. *Nat. Chem.* **2022**, *14*, 321−327.
(141) Alstrum-Acevedo, J. H.; Brennaman, M. K.; Meyer, T. J. Chemical Approaches to Artificial Photosynthesis. 2. *Inorg. Chem.* **2005**, *44*, 6802−6827.
(142) Liu, C.; Bos, D.; Hartog, B.; Meij, D.; Ramakrishnan, A.; Bonnet, S. Ligand Controls the Activity of Light-Driven Water Oxidation Catalyzed by Nickel(II) Porphyrin Complexes in Neutral Homogeneous Aqueous Solutions. *Angew. Chem., Int. Ed.* **2021**, *60*, 13463−13469.
(143) Ponseca, C. S., Jr.; Chábera, P.; Uhlig, J.; Persson, P.; Sundström, V. Ultrafast Electron Dynamics in Solar Energy Conversion. *Chem. Rev.* **2017**, *117*, 10940−11024.
(144) Saito, D.; Yamazaki, Y.; Tamaki, Y.; Ishitani, O. Photocatalysis of a Dinuclear Ru(II)-Re(I) Complex for CO_2 Reduction on a Solid Surface. *J. Am. Chem. Soc.* **2020**, *142*, 19249−19258.
(145) Neumann, S.; Kerzig, C.; Wenger, O. S. Quantitative insights into charge-separated states from one- and two-pulse laser experiments relevant for artificial photosynthesis. *Chem. Sci.* **2019**, *10*, 5624−5633.
(146) Watanabe, T.; Honda, K. Measurement of the Extinction Coefficient of the Methyl Viologen Cation Radical and the Efficiency of Its Formation by Semiconductor Photocatalysis. *J. Phys. Chem.* **1982**, *86*, 2617−2619.
(147) Kavarnos, G. J.; Turro, N. J. Photosensitization by reversible electron transfer: theories, experimental evidence, and examples. *Chem. Rev.* **1986**, *86*, 401−449.
(148) Troian-Gautier, L.; Swords, W. B.; Meyer, G. J. Iodide Photoredox and Bond Formation Chemistry. *Acc. Chem. Res.* **2019**, *52*, 170−179.
(149) Miedlar, K.; Das, P. K. Tris(2,2'-bipyridine)ruthenium(II)-Sensitized Photooxidation of Phenols. Environmental Effects on Electron Transfer Yields and Kinetics. *J. Am. Chem. Soc.* **1982**, *104*, 7462−7469.
(150) Georgopoulos, M.; Hoffman, M. Z. Cage Escape Yields In the Quenching of $*Ru(bpy)_3^{2+}$ by Methylviologen. Presence of Triethanolamine as a Sacrificial Electron Donor. *J. Phys. Chem.* **1991**, *95*, 7717−7721.
(151) Adams, R. E.; Schmehl, R. H. Micellar Effects on Photoinduced Electron Transfer in Aqueous Solutions Revisited: Dramatic Enhancement of Cage Escape Yields in Surfactant Ru(II) Diimine Complex/$[Ru(NH_3)_6]^{2+}$ Systems. *Langmuir* **2016**, *32*, 8598−8607.
(152) Neumann, S.; Wenger, O. S.; Kerzig, C. Controlling Spin-Correlated Radical Pairs with Donor Acceptor Dyads: A New Concept to Generate Reduced Metal Complexes for More Efficient Photocatalysis. *Chem.—Eur. J.* **2021**, *27*, 4115−4123.
(153) Henke, W. C.; Otolski, C. J.; Moore, W. N. G.; Elles, C. G.; Blakemore, J. D. Ultrafast Spectroscopy of $[Mn(CO)_3]$ Complexes: Tuning the Kinetics of Light-Driven CO Release and Solvent Binding. *Inorg. Chem.* **2020**, *59*, 2178−2187.
(154) Farrell, I. R.; Matousek, P.; Towrie, M.; Parker, A. W.; Grills, D. C.; George, M. W.; Vlček, A. Direct Observation of Competitive Ultrafast CO Dissociation and Relaxation of an MLCT Excited State: Picosecond Time-Resolved Infrared Spectroscopic Study of $[Cr(CO)_4$(2,2'-bipyridine)]. *Inorg. Chem.* **2002**, *41*, 4318−4323.
(155) Kottelat, E.; Lucarini, F.; Crochet, A.; Ruggi, A.; Zobi, F. Correlation of MLCTs of Group 7 fac-$[M(CO)_3]^+$ Complexes (M = Mn, Re) with Bipyridine, Pyridinylpyrazine, Azopyridine, and Pyridin-2-ylmethanimine Type Ligands for Rational photoCORM Design. *Eur. J. Inorg. Chem.* **2019**, *2019*, 3758−3768.
(156) Ford, P. C. From curiosity to applications. A personal perspective on inorganic photochemistry. *Chem. Sci.* **2016**, *7*, 2964−2986.
(157) Vaidyalingam, A.; Dutta, P. K. Analysis of the Photodecomposition Products of $Ru(bpy)_3^{2+}$ in Various Buffers and upon Zeolite Encapsulation. *Anal. Chem.* **2000**, *72*, 5219−5224.
(158) Dixon, I. M.; Heully, J.-L.; Alary, F.; Elliott, P. I. P. Theoretical illumination of highly original photoreactive ^{3}MC states and the mechanism of the photochemistry of Ru(II) tris(bidentate) complexes. *Phys. Chem. Chem. Phys.* **2017**, *19*, 27765−27778.
(159) Lameijer, L. N.; van de Griend, C.; Hopkins, S. L.; Volbeda, A.-G.; Askes, S. H. C.; Siegler, M. A.; Bonnet, S. Photochemical Resolution of a Thermally Inert Cyclometalated Ru(phbpy)(N-N)(Sulfoxide)$^+$ Complex. *J. Am. Chem. Soc.* **2019**, *141*, 352−362.
(160) Vittardi, S. B.; Thapa, R. M.; Breen, D. J.; Rack, J. J. A Future Perspective on Phototriggered Isomerizations of Transition Metal Sulfoxides and Related Complexes. *J. Am. Chem. Soc.* **2021**, *143*, 526−537.
(161) Ashford, D. L.; Glasson, C. R. K.; Norris, M. R.; Concepcion, J. J.; Keinan, S.; Brennaman, M. K.; Templeton, J. L.; Meyer, T. J. Controlling ground and excited state properties through ligand changes in ruthenium polypyridyl complexes. *Inorg. Chem.* **2014**, *53*, 5637−5646.
(162) Prier, C. K.; Rankic, D. A.; MacMillan, D. W. C. Visible light photoredox catalysis with transition metal complexes: applications in organic synthesis. *Chem. Rev.* **2013**, *113*, 5322−5363.
(163) Shi, S.; Jung, M. C.; Coburn, C.; Tadle, A.; Sylvinson, D.; Djurovich, P. I.; Forrest, S. R.; Thompson, M. E. Highly Efficient Photo- and Electroluminescence from Two-Coordinate Cu(I) Complexes Featuring Nonconventional N-Heterocyclic Carbenes. *J. Am. Chem. Soc.* **2019**, *141*, 3576−3588.
(164) Bizzarri, C.; Spuling, E.; Knoll, D. M.; Volz, D.; Bräse, S. Sustainable metal complexes for organic light-emitting diodes (OLEDs). *Coord. Chem. Rev.* **2018**, *373*, 49−82.
(165) Bilger, J. B.; Kerzig, C.; Larsen, C. B.; Wenger, O. S. A Photorobust Mo(0) Complex Mimicking $[Os(2,2'\text{-bipyridine})_3]^{2+}$ and Its Application in Red-to-Blue Upconversion. *J. Am. Chem. Soc.* **2021**, *143*, 1651−1663.
(166) Büldt, L. A.; Guo, X.; Vogel, R.; Prescimone, A.; Wenger, O. S. A Tris(diisocyanide)chromium(0) Complex Is a Luminescent Analog of Fe(2,2'-Bipyridine)$_3^{2+}$. *J. Am. Chem. Soc.* **2017**, *139*, 985−992.
(167) Wegeberg, C.; Häussinger, D.; Wenger, O. S. Pyrene-Decoration of a Chromium(0) Tris(diisocyanide) Enhances Excited State Delocalization: A Strategy to Improve the Photoluminescence of $3d^6$ Metal Complexes. *J. Am. Chem. Soc.* **2021**, *143*, 15800−15811.
(168) Wegeberg, C.; Wenger, O. S. Luminescent chromium(0) and manganese(I) complexes. *Dalton Trans.* **2022**, *51*, 1297−1302.
(169) Herr, P.; Kerzig, C.; Larsen, C. B.; Häussinger, D.; Wenger, O. S. Manganese(I) complexes with metal-to-ligand charge transfer luminescence and photoreactivity. *Nat. Chem.* **2021**, *13*, 956−962.
(170) Lowry, M. S.; Bernhard, S. Synthetically tailored excited states: phosphorescent, cyclometalated iridium(III) complexes and their applications. *Chem.—Eur. J.* **2006**, *12*, 7970−7977.
(171) Duchanois, T.; Etienne, T.; Cebrián, C.; Liu, L.; Monari, A.; Beley, M.; Assfeld, X.; Haacke, S.; Gros, P. C. An Iron-Based Photosensitizer with Extended Excited-State Lifetime: Photophysical and Photovoltaic Properties. *Eur. J. Inorg. Chem.* **2015**, *2015*, 2469−2477.
(172) Liu, Y.; Harlang, T.; Canton, S. E.; Chábera, P.; Suárez-Alcántara, K.; Fleckhaus, A.; Vithanage, D. A.; Göransson, E.; Corani, A.; Lomoth, R.; Sundström, V.; Wärnmark, K. Towards longer-lived metal-to-ligand charge transfer states of iron(II) complexes: an N-heterocyclic carbene approach. *Chem. Commun.* **2013**, *49*, 6412−6414.
(173) Kunnus, K.; Guo, M.; Biasin, E.; Larsen, C. B.; Titus, C. J.; Lee, S. J.; Nordlund, D.; Cordones, A. A.; Uhlig, J.; Gaffney, K. J. Quantifying the Steric Effect on Metal-Ligand Bonding in Fe Carbene Photosensitizers with Fe 2p3d Resonant Inelastic X-ray Scattering. *Inorg. Chem.* **2022**, *61*, 1961−1972.
(174) Ashley, D. C.; Jakubikova, E. Tuning the Redox Potentials and Ligand Field Strength of Fe(II) Polypyridines: The Dual π-Donor and

https://doi.org/10.1021/jacs.2c02592
J. Am. Chem. Soc. 2022, 144, 9859−9873

π-Acceptor Character of Bipyridine. *Inorg. Chem.* **2018**, *57*, 9907−9917.

https://doi.org/10.1021/jacs.2c02592
J. Am. Chem. Soc. 2022, 144, 9859−9873